Multifidelity Bayesian Sequential Optimization and Reliability Assessment for Aerospace Systems Design

Romain Espoeys,* Loic Brevault,† and Mathieu Balesdent‡
ONERA, Paris Saclay University, 91120 Palaiseau, France
and
Sophie Ricci§ and Paul Mycek¶
CERFACS/CNRS UMR 5318, 31100 Toulouse, France

https://doi.org/10.2514/1.I011614

The design of aerospace systems requires the use of computationally intensive numerical solvers. Most often, the designer has access to simulation codes with different levels of fidelity, characterized by different accuracy and computational cost. In addition, certain phenomena manifest a stochastic nature that needs to be accounted for in the design process. Incorporating multiple sources of uncertainty through reliability-based design optimization (RBDO) then becomes a challenging task. Among the potential strategies, decoupled approaches such as SORA iterate between deterministic optimization and reliability analysis. However, when employing high-fidelity solvers, such methods still induce significant computational burdens. A way to further alleviate the computational cost issues is to involve models of fidelity throughout the RBDO problem. In this paper, a Bayesian approach with multifidelity surrogate models is proposed to tackle the optimization problems within SORA. This approach facilitates the incorporation of additional sources of information provided by lower fidelity models. Furthermore, the surrogate models are built in an augmented space allowing to reuse information along the RBDO iterations. The efficiency of the proposed framework is compared to reference approaches on four test cases with increasing complexity, and two aerospace realistic cases concerning the optimization of a solid-propellant rocket booster and a sounding rocket.

I. Introduction

NUMEROUS deterministic optimization (DO) methods have emerged in the literature to address the design of aerospace vehicles, whose behavior is classically described by simulation codes that can be coupled into a multidisciplinary process [1–3]. These methods offer the possibility of increasing the performance of the system while reducing its overall cost. However, certain variables or phenomena exhibit a stochastic nature that should be taken into account in the optimization process. For instance, the appearance of wind gusts during a launch vehicle flight should be considered in the design process of the launcher [4]. This can be addressed by employing reliability-based design optimization (RBDO) methods [5,6]. In RBDO approaches, a reliability analysis (RA) is involved in the optimization process in order to estimate the probability of failure of the system considering the values of the design variables. In the presence of uncertainty, the inequality constraints in the optimization problem are usually considered under the form of a probability of failure.

Classically, uncertainties are classified into two categories: aleatory and epistemic. In the context of RBDO, aleatory variables are further divided into controlled or uncontrolled variables according to their roles in the optimization process. The controlled uncertain variables are modeled by random variables with prescribed probability density functions (PDFs), whose hyperparameters (e.g., mean value) are considered as design variables. On the other hand, the uncontrolled uncertain variables may reflect the stochastic effects in the system environment. For example, in an aerospace problem, design variables can be the diameter of the rocket and the propellant mass. Due to the fueling operation (e.g., leaks, cryogenic propellant evaporation), it is possible to consider the onboard propellant mass at the moment of liftoff as a random variable. The nominal value of the propellant mass may be considered as a controlled variable representing a specification that is optimized. It corresponds to the expected value of the onboard propellant mass random variable. An example of an uncontrolled uncertain variable can be wind gusts during the flight of the rocket.

A pragmatic way to solve such an optimization problem in the presence of uncertainty is to adopt a two-level strategy [7]. All the functions impacted by the uncertain variables (objective function, constraint functions) involve an uncertainty measure such as an expected value, a quantile, a variance, or a probability of failure. In the two-level approach, the outer loop solves the DO problem, while the inner loop corresponds to the reliability analysis for the current design variable values provided by the optimizer algorithm. The estimation of the probability of failure P_f, which may be formulated as a multidimensional integral, requires numerous calls to the simulation code, especially when P_f is low (e.g., 10^{-4}). Consequently, this approach is not affordable in practice for computationally intensive solvers.

Several other approaches have been proposed in order to reduce the number of RAs during the RBDO process [8,9], with applications to aerospace design [10]. By reducing the number of RAs during the optimization process, the goal of these techniques is to reduce the computational cost by avoiding unnecessary costly RAs. Among them, the single-level approaches combine the two loops into a single one [8] by replacing the probabilistic constraints by equivalent optimal conditions through a Lagrangian formulation. In the decoupled approaches, the nested structure of classical approaches is reformulated as a sequence of two loops, respectively, dedicated to the resolution of an equivalent DO problem and the resolution of an RA problem [9]. Although these approaches succeed in alleviating the computational burden of the RA during the optimization, they introduce approximations. Among the decoupled approaches, the sequential optimization and reliability assessment (SORA) method solves the RA using the inverse first-order reliability method (inverse FORM, also called the performance measure approach) [7,11–13]. The FORM technique consists of performing a linear approximation of the limit state at the most probable failure

Received 21 January 2025; accepted for publication 15 July 2025; published online 2 September 2025.

*Ph.D. Student, ONERA DTIS, CERFACS CECI; also CERFACS/CNRS UMR, 5318 Toulouse, France; espoeysromain@gmail.com (Corresponding Author).
†Research Engineer, DTIS; loic.brevault@onera.fr.
‡Research Director, DTIS; mathieu.balesdent@onera.fr.
§Research Director, CECI; ricci@cerfacs.fr.
¶Research Engineer, CECI; mycek@cerfacs.fr.

point associated with the constraint function in order to analytically compute the probability of failure. Conversely, the inverse FORM technique aims at finding the minimum performance target point of the aleatory vector consistent with the target probability of failure. However, when dealing with computationally expensive solvers, the number of required evaluations of the high-fidelity code may still be prohibitive for SORA. An efficient way of reducing the computational cost is to replace the expensive solvers with surrogate models. In the literature, some methods have been proposed to replace only the constraints with surrogate models [14,15]. Other approaches substitute both the objective function and the constraint functions [6,16–18] with surrogate models.

Gaussian processes (GPs) [19,20] are usually employed in the literature to construct surrogate models. These probabilistic models are defined by a mean function and a covariance function. A GP, once trained on a dataset, provides a prediction model and an associated confidence model (uncertainty model) [20,21]. This confidence model quantifies the epistemic uncertainty linked to the construction of the surrogate model, which decreases as the database grows. In the context of reliability analysis, GPs have been widely used with different sampling schemes [22], such as Monte Carlo simulation, importance sampling, and subset simulation, combined with a variety of active learning strategies (e.g., *U*-criterion [23], expected feasibility function [24], stepwise uncertainty reduction [25], fraction of bootstrap replicate [26]). The goal is to refine the surrogate model only near the limit state function while ensuring the confidence level of the estimation of the probability of failure. For more details, one can consult [27].

Furthermore, GPs have also been introduced to solve RBDO problems [6,16,17,28,29]. In the context of RBDO using Bayesian optimization, surrogate models of the objective and constraint functions are built from a limited dataset and then iteratively enriched in regions of interest using a dedicated infill criterion. These regions correspond to locations with a high likelihood of finding the global minimum of the objective function while satisfying the probabilistic constraints. The infill criterion is based on the GP prediction and associated confidence level. Traditionally, when tackling RBDO problems, surrogate models are either built in the design variable space or in the uncertain variable space. To improve the RBDO solving efficiency, it has been proposed to construct the surrogates in an *augmented space* combining the uncertain and the design spaces [6,30], defined as the Cartesian product of both definition domains. It offers the possibility to reuse information throughout the DO and RA iterations in SORA and consequently to speed up the optimization process. However, this approach may lead to a significant increase in the dimension of the input space and may limit the accuracy of the surrogate models. Therefore, a large number of high-fidelity model evaluations may be required to obtain accurate surrogate models, at the expense of the computational cost.

Leveraging lower-fidelity solvers allows us to furnish supplementary information for constructing the surrogate models at a significantly lower computational cost but with a reduced accuracy compared to high-fidelity solvers. These multiple sources of information can be aggregated into a multifidelity surrogate model. This results in the introduction of additional epistemic uncertainties linked to levels of fidelity. For instance, in the case of an aerospace vehicle, the aerodynamic performance may be estimated using a computational fluid dynamics, Reynolds-averaged Navier–Stokes (CFD RANS) code that may be considered as high-fidelity compared to a low-fidelity model such as CFD Euler. Several multifidelity techniques based on GPs have been reported in the literature [31–33]. One of the most popular methods is the autoregressive model (AR1) [32], also known as cokriging. This technique is particularly relevant when the outputs of the different fidelity levels present linear dependencies [34]. Associated work has also been carried out to extend this method to multi-output problems [35]. Multifidelity techniques have been used for Bayesian optimization purposes [36–39]. Bayesian optimization is suited to perform global optimization in a context of numerically costly models. The advantage of Bayesian optimization is to start from a limited database and compute the expensive model only where it is helpful in order to solve the optimization problem. Indeed, through a dedicated active learning process, the simulation codes are only evaluated on interesting regions regarding either the potential location of the minimum (for the optimization purpose) or the limit state function (for the reliability analyses), thus limiting the overall computational budget.

In the literature, some techniques have been developed to take advantage of lower fidelity information sources in an RBDO context [40–42] to reduce the computational cost by reusing information from multiple fidelity levels. In [40], a method is detailed using the results of previous RBDO iterations near the current design point to build low-fidelity models for the reliability analysis. However, this approach does not handle problems with several levels of fidelity. It only allows the reuse of a single-fidelity surrogate model of the constraint function built during previous iterations as a low-fidelity source of information within the framework of a reliability analysis using the mfEGRA method [43]. It therefore does not provide a multifidelity active learning framework to solve RBDO problems. In [42], an iterative scheme involving two phases (multifidelity model enrichment and RBDO) is proposed. In this approach, multifidelity models of the constraint functions are built in an offline phase and then used for RBDO. Once the RBDO has been performed, the surrogate models are then updated with the optimal solution found by the RBDO. However, as this approach is based on an offline construction of constraint surrogate models for a given design point (i.e., not in a global augmented space), it does not enable the reuse of information throughout the optimization process. In [41], a sequential strategy based on multifidelity artificial neural networks is described in which the surrogate models are built to solve the RBDO problem. Monte Carlo, FORM, or second-order reliability method (SORM) are then used to compute the failure probabilities. While this method benefits from multifidelity source aggregation, it does not propose an in-line active-learning strategy included in the RBDO process. Furthermore, the construction of surrogate models is not done in an augmented space of design and uncertain variables, which prevents information from being reused. Moreover, in [40–42], the authors do not propose a strategy for building a surrogate model of the objective function directly during the RBDO process. In addition, they mostly rely on double-loop approaches and do not benefit from the Bayesian optimization scheme to solve the RBDO process. In [44], a multifidelity RBDO strategy based on SORA is introduced. The authors couple an adaptive solving strategy and a surrogate model local update framework with a dedicated judgment criterion to target the active constraints. However, this method only focuses on the treatment of controlled uncertain variables and does not propose an active learning strategy for design and uncontrolled uncertain parameters.

In this article, a decoupled RBDO approach combined with multifidelity and active-learning strategy for GPs is proposed, hereafter referred to as multifidelity Bayesian SORA (MFB-SORA). The contribution of this paper is to propose a new RBDO methodology combining Bayesian optimization, the use of augmented space for active learning. and multifidelity Gaussian processes. This method relies on a decoupled scheme based on SORA framework. The surrogate models are constructed in the augmented space by active learning during the different optimization processes of the SORA framework (deterministic optimization and reliability analyses formulated as an optimization problem through inverse FORM). Multifidelity Bayesian optimization is used to solve the optimization processes by reusing the information contained in the multifidelity databases constructed in the joint space of uncertain and design parameters.

The outline of the paper is as follows: Section II presents a brief state-of-the-art of RBDO techniques and multifidelity Bayesian optimization approaches using Gaussian processes. Section II.A describes the formulation of the RBDO problem and briefly details existing approaches to solve such problems. Then, the construction of the augmented space is presented. In Sec. II.B, Bayesian optimization in the context of multifidelity is briefly introduced. Section III details the proposed RBDO approach derived from SORA based on multifidelity Bayesian optimization in the augmented

space. Numerical experiments are conducted in Sec. IV to compare the proposed innovative approach with classical techniques such as the two-level approach and the classical SORA. A total of five test cases are presented in this article: three analytical cases and two physical aerospace application cases. Among the analytical cases, one concerns a vehicle brake disk [42,45] and an aerospace speed reducer [46,47]. The physical aerospace cases concern the optimization of a solid-propellant rocket booster and the optimization of a sounding rocket.

II. State-of-the-Art

A. Reliability-Based Design Optimization (RBDO)

1. Problem Formulation

The adaptation of a deterministic optimization problem in the presence of uncertain variables gives rise to a reliability-based design optimization (RBDO) problem [5]. In this context, the inequality constraints are formulated as probabilities of failure. The probabilistic constraints are evaluated using reliability analysis (RA).

In the following, the formulation adopted in [9,48] is employed. Two types of design variable vectors may be distinguished: the classical deterministic design variable vector of size n_d, and the design variable vector $\boldsymbol{p} \in \mathbb{R}^{n_p}$ associated with the *controlled* uncertain variable vector $\boldsymbol{X}$ of size $n_X = n_p$. It corresponds to some of the hyperparameters defining the joint probability density function (PDF) of $\boldsymbol{X}$ (for instance, the mean value). The vector of aleatory variables $\boldsymbol{X}$ is *controlled* by the design vector $\boldsymbol{p}$. Each component X_i of $\boldsymbol{X}$ for $i \in \{1, \ldots, n_p\}$ is distributed according to the marginal distribution with PDF $\phi_{X_i|p_i}$ (e.g., a normal distribution), where p_i is the mean of the distribution (e.g., the mean of the normal distribution). The *uncontrolled* variables reflect the stochastic nature of the system or its environment. They are gathered in the vector $\boldsymbol{Z}$ characterized by its PDF $\phi_{\boldsymbol{Z}}$.

For instance, in the context of aerospace vehicle design, an example of a deterministic design variable d is the rocket stage diameter. A design variable p may represent the specification of the mass of cryogenic propellant onboard of a rocket tank. However, due to fueling operations that are stochastic (due to leaks and propellant evaporation), the final propellant mass at liftoff is uncertain. Therefore, such a variable may be modeled with a Gaussian random variable $X \sim \mathcal{N}(p, \sigma_X^2)$ in which p is the propellant mass specification that is optimized and σ_X^2 is the propellant mass variance related to fueling operation. An uncontrolled uncertainty $Z \sim \mathcal{N}(\mu_Z, \sigma_Z^2)$ may represent the presence of wind gusts during the rocket's flight, modeled by a Gaussian distribution with mean μ_Z representing the average intensity of wind gusts, and σ_Z^2 its variance.

The objective function depends, respectively, on n_d and n_p deterministic design variables gathered in the vectors $\boldsymbol{d}$ and $\boldsymbol{p}$. The failure of the constraint function $g_i(\cdot)$ occurs when $g_i(\boldsymbol{d}, \boldsymbol{X}(\boldsymbol{p}), \boldsymbol{Z}) \leqslant 0$ (for $i \in \{1, \ldots, n_g\}$ and without loss of generality). The constraint function $g_i(\cdot)$ depends on the design variable vector $\boldsymbol{d}$, on the *controlled* aleatory variable vector $\boldsymbol{X}$ (modified in the optimization process through the design vector $\boldsymbol{p}$) as well as on the *uncontrolled* vector $\boldsymbol{Z}$. The optimal solution $(\boldsymbol{d}_*, \boldsymbol{p}_*)$ of the RBDO problem ensures that the probability of failure (associated with the constraints) remains below a prescribed target value $P_{f,i}^t$, i.e., $\mathbb{P}[g_i(\boldsymbol{d}_*, \boldsymbol{X}(\boldsymbol{p}_*), \boldsymbol{Z}) \leqslant 0] \leqslant P_{f,i}^t$ for $i \in \{1, \ldots, n_g\}$. In the following, for the sake of simplicity, deterministic constraints do not appear in the problem formulation. The RBDO problem is formulated as

$$\min_{\boldsymbol{d},\boldsymbol{p}} f(\boldsymbol{d}, \boldsymbol{p}) \quad \text{s.t.} \begin{cases} \mathbb{P}[g_i(\boldsymbol{d}, \boldsymbol{X}(\boldsymbol{p}), \boldsymbol{Z}) \leqslant 0] \leqslant P_{f,i}^t & \text{for } i = 1, \ldots, n_g \\ \boldsymbol{d}^- \leqslant \boldsymbol{d} \leqslant \boldsymbol{d}^+ \\ \boldsymbol{p}^- \leqslant \boldsymbol{p} \leqslant \boldsymbol{p}^+ \end{cases} \tag{1}$$

where $\boldsymbol{d}^-, \boldsymbol{d}^+ \in \mathbb{R}^{n_d}$ and $\boldsymbol{p}^-, \boldsymbol{p}^+ \in \mathbb{R}^{n_p}$ are the bounds of the optimization variables, and $f(\cdot)$ is the deterministic objective function to be minimized. The optimization problem is associated with n_g probabilistic constraints $g_i(\cdot)$, for $i = 1, \ldots, n_g$. The *limit state surface* of the constraint function $g_i(\cdot)$ is defined by the set of triplets $(\boldsymbol{d}, \boldsymbol{X}, \boldsymbol{Z})$ such that $g_i(\boldsymbol{d}, \boldsymbol{X}, \boldsymbol{Z}) = 0$. Several strategies to solve the introduced RBDO problem are briefly presented in the next section.

2. RBDO Approaches

Various techniques to solve RBDO problems of the form (Eq. 1) are reported in the literature [5,6]. Four classes may be distinguished and are represented in Fig. 1: the *two-level approaches* [7,49], the *single-level approaches* [8], the *decoupled approaches* [9], and the *surrogate model-based approaches* [6,16,17].

The most direct technique is the *two-level approach*, characterized by a nested structure: the outer loop addresses the optimization problem, while the inner one conducts the RA for each probabilistic constraint. In practice, the most intuitive method for evaluating a probability of failure involves the numerical approximation of the associated multivariate integral, using sampling approaches such as Monte Carlo (MC) simulation [50]. Due to the central limit theorem, when the probability of failure is low (below 10^{-4}), a large number of model evaluations is required to obtain an accurate estimate, incurring a substantial computational cost. To overcome these limitations, the reliability index approach (RIA) [49] has been proposed, based on the FORM [11,12] for RA. FORM relies on a linear approximation of the limit state surface at the most probable failure point (MPFP), which provides a closed-form (analytic) expression of the resulting (approximate) probability of failure. RA then consists in locating the MPFP in the standard normal space by solving an auxiliary optimization problem involving the constraint function $g_i(\cdot)$. Alternatively, the performance measure approach (PMA) [7] has been proposed to further simplify the auxiliary optimization problem using inverse FORM [13]. The goal of PMA is to identify the minimum performance target point (MPTP), i.e., the point with the minimum constraint value that complies with the target probability. This is achieved by solving an auxiliary optimization problem that is more tractable (due to the constraint expression) than the one required to identify the MPFP [5,51].

The *single-level approach* (or *single-loop approach*) modifies the initial RBDO formulation to include RA within the optimization

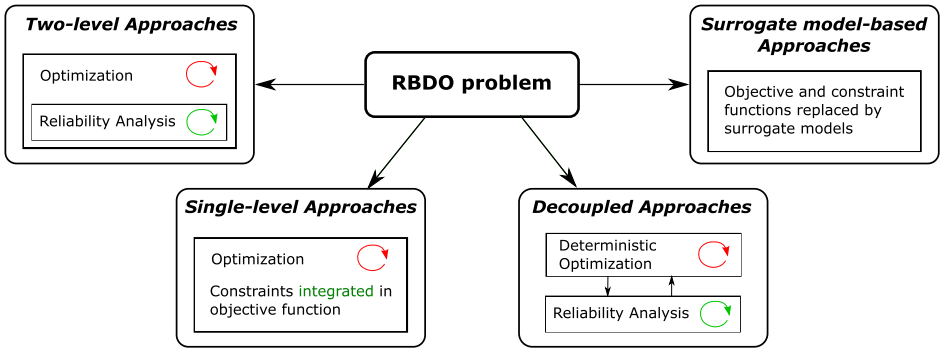

Fig. 1 Families of approach for RBDO problems. The red loop refers to the optimization, whereas the green loop refers to the reliability analysis for the constraints.

problem. The RBDO problem is reformulated as a problem without RA, by replacing the probabilistic constraints by equivalent optimal conditions (for instance, based on Karush–Kuhn–Tucker optimality conditions [52]) through a Lagrangian formulation. The new deterministic optimization problem is then solved in a single-loop procedure, by minimizing the objective function while implicitly respecting the constraints. Following this strategy, Liang et al. developed the single-loop approach [8].

The *decoupled approach* splits the optimization part and the RA to reduce the overall number of RAs. In the SORA strategy [9], the RBDO problem is solved through an iterative procedure involving a sequence of two specific steps. First, an equivalent DO problem with respect to the design variable vectors $\boldsymbol{d}$ and $\boldsymbol{p}$ is solved. In this problem, the probabilistic constraints are replaced by equivalent deterministic constraints, in which the aleatory variables are shifted by a certain distance consistent with the target probability of failure P_f^t in the standard normal space. The introduction of the shifting vectors allows us to solve the DO problem in a region, most likely leading to feasible probabilistic constraints. Then, for the design variable vectors $\boldsymbol{d}$ and $\boldsymbol{p}$ fixed to the optimal values found in DO, for each probabilistic constraint, RA is performed using an inverse FORM approach. After the RA, the shifting vectors are updated based on the reliability results and the current optimum obtained at the previous DO. The next DO problem is then solved with the updated shifting vectors.

The last family of techniques, known as the *surrogate model-based approaches* [6,16,17,28], aims at reducing the computational cost of the RBDO process by substituting the objective and constraint functions by surrogate models. These approximate models are built from a database of simulations called the training dataset. This dataset can be constructed from a large design of experiments (DoEs). Then, after a training procedure, the metamodels can be used instead of the exact functions to solve the RBDO problem. However, this offline approach may provide poor results. An alternative strategy consists of starting from a small-sized DoE, and then adding new data points valuable for the optimization and reliability tasks. These new samples are selected according to infill criteria (either for the optimization or for the reliability analysis) during an online procedure.

Several sampling techniques can be used to generate the initial DoE, such as Monte Carlo [50], following an a *priori* random distribution. Most often, space-filling designs are preferred in order to evenly distribute the data points in the design space. Classical techniques [53] comprise Halton or Sobol' sequences, Latin hypercube sampling (LHS), optimized LHS, etc. The choice of the sampling method is critical for surrogate modeling in an offline approach. In this work, it is chosen to generate the initial DoE with an LHS.

The reorganization of the optimization and reliability steps in the single-loop and decoupled approaches lowers the RBDO computational costs compared to the two-level approaches [5,6]. Nevertheless, these approaches may remain unaffordable for high-fidelity models and surrogate models should be used. In the present paper, the proposed approach consists in combining the decoupled SORA technique with multifidelity Bayesian optimization based on surrogate models built in an augmented space. In the following section, a more detailed presentation of SORA is given.

3. Sequential Optimization and Reliability Assessment (SORA)

Under some hypotheses of linear approximation of the limit state functions at the MPFP and the existence of a single MPFP by probabilistic constraint [9], SORA defines an equivalent problem formulation to the RBDO problem (1):

$$\min_{\boldsymbol{d},\boldsymbol{p}} f(\boldsymbol{d},\boldsymbol{p}) \quad \text{s.t.} \begin{cases} g_i(\boldsymbol{d},\boldsymbol{x}_{\text{MPTP},i},\boldsymbol{z}_{\text{MPTP},i}) \geqslant 0 \quad \text{for } i=1,\dots,n_g \\ \boldsymbol{d}^- \leqslant \boldsymbol{d} \leqslant \boldsymbol{d}^+ \\ \boldsymbol{p}^- \leqslant \boldsymbol{p} \leqslant \boldsymbol{p}^+ \end{cases} \tag{2}$$

where $g_i^t = g_i(\boldsymbol{d},\boldsymbol{x}_{\text{MPTP},i},\boldsymbol{z}_{\text{MPTP},i})$ denotes the R-percentile of $g(\boldsymbol{d},\boldsymbol{X}(\boldsymbol{p}),\boldsymbol{Z})$ with $R = P_{f,i}^t$, i.e., such that $\mathbb{P}[g_i(\boldsymbol{d},\boldsymbol{X}(\boldsymbol{p}),\boldsymbol{Z}) \leqslant g_i^t] = P_{f,i}^t$, for $i = 1,\dots,n_g$. Note that $\boldsymbol{x}_{\text{MPTP},i}$ and $\boldsymbol{z}_{\text{MPTP},i}$ stand for the MPTP values of the random vectors $\boldsymbol{X}$ and $\boldsymbol{Z}$, i.e., the critical values leading to the target probability of failure $P_{f,i}^t$. By introducing the mean parameter vector $\boldsymbol{p}$ of the joint distribution of the random vector $\boldsymbol{X}$, it is possible to rewrite the deterministic constraint of Eq. (2) such that $g(\boldsymbol{d},\boldsymbol{p}-\boldsymbol{s}_i,\boldsymbol{z}_{\text{MPTP},i}) \geqslant 0$, for $i = 1,\dots,n_g$, where $\boldsymbol{s}_i = \boldsymbol{p} - \boldsymbol{x}_{\text{MPTP},i}$ stands for the shifting vector leading to the feasible region of the constraint i. In the SORA framework, the key idea is to solve this equivalent deterministic optimization problem by fixing the shifting vector $\boldsymbol{s}_i$ and $\boldsymbol{z}_{\text{MPTP},i}$ at values provided by the previous SORA iteration.

For the first SORA iteration ($k = 0$), the n_g shifting vectors $\boldsymbol{s}_i^{(0)}$ are initialized to zero and the MPTP $\boldsymbol{z}_{\text{MPTP},i}^{(0)}$ are set to the mean value $\boldsymbol{\mu}_Z$ of the random vector $\boldsymbol{Z}$. Then, at the kth iteration of SORA, for each DO phase, for each constraint $i = 1,\dots,n_g$, the aleatory variables $\boldsymbol{Z}$ are fixed at their current MPTP value $\boldsymbol{z}_{\text{MPTP},i}^{(k)}$. The mean values $\boldsymbol{p}$ of the controlled design uncertain variables $\boldsymbol{X}$ are shifted by the shifting vector value $\boldsymbol{s}_i^{(k)}$, defined as the distance to the point that leads to $P_{f,i}^t$, based on $\boldsymbol{x}_{\text{MPTP},i}^{(k)}$. At the kth iteration of SORA, the solution of the DO problem is defined as

$$\boldsymbol{d}_*^{(k)},\boldsymbol{p}_*^{(k)} = \underset{\boldsymbol{d},\boldsymbol{p}}{\operatorname{argmin}}\ f(\boldsymbol{d},\boldsymbol{p}) \quad \text{s.t.} \begin{cases} g_i(\boldsymbol{d},\boldsymbol{p}-\boldsymbol{s}_i^{(k)},\boldsymbol{z}_{\text{MPTP},i}^{(k)}) \geqslant 0 \quad \text{for } i=1,\dots,n_g. \\ \boldsymbol{d}^- \leqslant \boldsymbol{d} \leqslant \boldsymbol{d}^+ \\ \boldsymbol{p}^- \leqslant \boldsymbol{p} \leqslant \boldsymbol{p}^+ \end{cases} \tag{3}$$

Considering the DO optimal point $(\boldsymbol{d}_*^{(k)},\boldsymbol{p}_*^{(k)})$, RA is formulated as an optimization problem in order to determine the MPTP values of the aleatory vectors $\boldsymbol{X}$ and $\boldsymbol{Z}$ using the inverse FORM approach:

$$\boldsymbol{u}_{\text{MPTP},i} = \underset{\boldsymbol{u}}{\operatorname{argmin}}\ G_i(\boldsymbol{d}_*^{(k)},\boldsymbol{u}) \quad \text{s.t.} \quad \|\boldsymbol{u}\| = \beta_i^t \quad \text{for } i=1,\dots,n_g \tag{4}$$

where $G_i(\boldsymbol{d},\boldsymbol{u}) = g_i(\boldsymbol{d},\mathcal{T}_{\boldsymbol{p}_*^{(k)}}^{-1}(\boldsymbol{u}))$. $\mathcal{T}_{\boldsymbol{p}_*^{(k)}}(\cdot)$ is the isoprobabilistic transformation that maps the vector formed by the concatenation of the vectors $\boldsymbol{X}$ and $\boldsymbol{Z}$ from their domain of definition (i.e., physical space) to a vector $\boldsymbol{U}$ in the standard normal space. This transformation depends on the optimal parameters $\boldsymbol{p}_*^{(k)}$ that describe the PDF of $\boldsymbol{X}$: $\boldsymbol{U} = \mathcal{T}_{\boldsymbol{p}_*^{(k)}}([\boldsymbol{X},\boldsymbol{Z}]^T) \sim \mathcal{N}(\boldsymbol{0},\boldsymbol{I})$, with $\boldsymbol{I}$ the identity matrix; β_i^t is the target distance related to $P_{f,i}^t$ by $\beta_i^t = -\Phi^{-1}(P_{f,i}^t)$, where $\Phi(\cdot)$ is the cumulative density function (CDF) of the standard normal distribution. The result of the inverse FORM optimization is mapped back onto the physical space. For the ith constraint, $[\boldsymbol{x}_{\text{MPTP},i}^{(k)},\boldsymbol{z}_{\text{MPTP},i}^{(k)}]^T = \mathcal{T}_{\boldsymbol{p}_*^{(k)}}^{-1}(\boldsymbol{u}_{\text{MPTP},i})$ is the MPTP in the physical space. For the next DO step, the random vector $\boldsymbol{Z}$ is set to the MPTP value $\boldsymbol{z}_{\text{MPTP},i}^{(k)}$, and the shifting vector is updated as

$$\boldsymbol{s}_i^{(k+1)} = \boldsymbol{p}_*^{(k)} - \boldsymbol{x}_{\text{MPTP},i}^{(k)} \tag{5}$$

DO and RA are iterated until convergence (stagnation of the DO optimal solution and stagnation of the shifting vectors) is reached, or until a specified stopping criterion is reached. The SORA algorithm for solving the RBDO problem defined in Eq. (1) is presented in Fig. 2.

4. Correction of the Shifting Vector Using Importance Sampling (IS)

One limitation of SORA is the use of inverse FORM for RA. This method estimates the probability of failure at the MPTP through a linear approximation of the limit state function. These approximations directly impact the estimation of the shifting vector. In order to

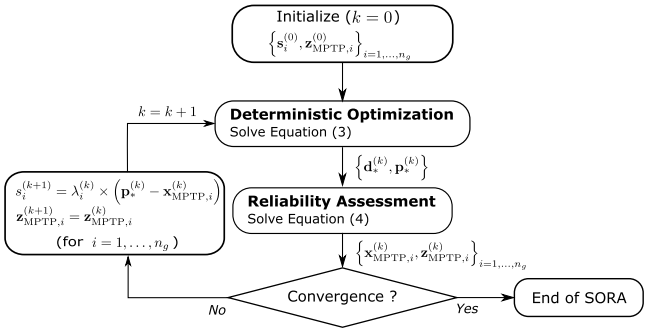

Fig. 2 Flowchart of SORA method.

further improve the SORA approach, a new definition of the shifting vector has been proposed in [48] based on an importance sampling (IS) [54] estimation of the failure probability. This estimation is performed using a surrogate model of the constraint function to avoid computational burden. IS improves the accuracy and efficiency of the probability calculation by introducing an auxiliary sampling density to target the failure zone. In the present paper, the shifting vector correction of [48] presented in this section is applied.

For each constraint function $g_i(\cdot)$, at iteration k, RA provides an MPTP point consistent with the target probability of failure $P_{f,i}^t$, corresponding to a target reliability index β_i^t, through a linear approximation of the limit state surface. However, this estimation is accurate only if the limit state surface can be approximated by a linear function and if a unique failure point exists. If it is not the case, the inaccuracy introduced at this stage directly impacts the shifting vector $\boldsymbol{s}_i^{(k)}$ computed from $\boldsymbol{x}_{\mathrm{MPTP},i}^{(k)}$. As introduced in [48], the surrogate model of each constraint function can be used to estimate by importance sampling the probability of failure $P_{f,i}^{\mathrm{IS}(k)}$ using an auxiliary density located at the MPTP. Then, the shifting vector can be adjusted by using a multiplicative factor $\lambda_i^{(k)}$:

$$\boldsymbol{s}_{i,\mathrm{corr}}^{(k+1)} = \lambda_i^{(k)} \boldsymbol{s}_i^{(k+1)} \tag{6}$$

where $\boldsymbol{s}_i^{(k+1)}$ is the classical shifting vector of SORA computed by Eq. (5), and $\lambda_i^{(k)}$ is formulated as the ratio between the target reliability index β_i^t and the estimated reliability index $\beta_i^{\mathrm{IS}(k)} = -\Phi^{-1}(P_{f,i}^{\mathrm{IS}(k)})$:

$$\lambda_i^{(k)} = \frac{\beta_i^t}{\beta_i^{\mathrm{IS}(k)}} \tag{7}$$

In [48], the construction of the surrogate models of the constraints is performed before the optimization process. It is thus driven neither by the optimization nor by the RA. The surrogate models are enriched over the entire input space, and not particularly around the optimum of the problem, which may lead to unnecessary high-fidelity model evaluations in regions far from the optimum. In this paper, an active learning process is proposed to enrich the surrogate model only in relevant zones with respect to the DO and RA problems.

5. Augmented Space Framework for Surrogate Model-Based RBDO Techniques

The use of surrogate models is a classical way to reduce computational cost in an RBDO framework. In SORA, the constraint functions $g_i(\cdot)$ are evaluated during both the DO and RA phases. The main difficulty when replacing them with surrogate models is thus to ensure the consistency of these surrogate models between the different phases of SORA. Indeed, during DO, the surrogate models of the constraint functions depend on the design variables $\boldsymbol{d}$ and $\boldsymbol{p}$, while $\boldsymbol{s}_{i,\mathrm{corr}}^{(k)}$ and $\boldsymbol{z}_{\mathrm{MPTP},i}^{(k)}$ are fixed to their current values determined at the previous SORA iteration. Conversely, during RA, the surrogate models of the constraint functions depend on the uncertain variables $\boldsymbol{X}$ and $\boldsymbol{Z}$, with fixed values of the design variable vectors $\boldsymbol{d}_*^{(k)}$ and $\boldsymbol{p}_*^{(k)}$.

Such surrogate models in SORA can be formulated with different approaches. If the surrogate models are rebuilt at each iteration and each stage of SORA, they are alternatively built in reduced space, considering constant values for $\{\boldsymbol{s}_{i,\mathrm{corr}}^{(k)}, \boldsymbol{z}_{\mathrm{MPTP},i}^{(k)}\}$ or $\{\boldsymbol{d}_*^{(k)}, \boldsymbol{p}_*^{(k)}\}$. However, this approach prevents reusing the surrogate model information between DO and RA steps as well as along iterations of SORA. A more efficient approach consists in considering the surrogate model of the constraint function $g_i(\cdot)$ (for $i = 1,\ldots,n_g$) for both DO and RA, in an *augmented space* [6,30] that spans both design and uncertain spaces. The idea behind such a space, as introduced by [30], is to artificially consider the set of design parameters as uncertain with a specified PDF in the case of an augmented reliability problem. In practice, this choice does not imply that the design vector is uncertain, since it represents a specification or a decision. Without loss of generality, it is assumed in this article that the considered random variables for the construction of the augmented space are independent. The augmented space is then constructed as the Cartesian product of the confidence region of each variable over both design and uncertain spaces.

For the design vector $\boldsymbol{d}$, it can be artificially assumed that each particular design variable follows a uniform distribution between its bounds. The resulting confidence region $\mathbb{D}$ is then simply defined by the Cartesian product of the interval bounds as

$$\mathbb{D} = \bigtimes_{i=1}^{n_d} [d_i^-, d_i^+] \tag{8}$$

with $\times$ the Cartesian product symbol. In SORA, the variables $\boldsymbol{p} \in [\boldsymbol{p}^-, \boldsymbol{p}^+]$ correspond to the mean vector of the distribution of $\boldsymbol{X}(\boldsymbol{p})$. A confidence region for such variables can be defined by the probability of sampling outside the definition area, denoted by α_{X_j}, at the lower and upper bounds p_j^- and p_j^+, for $j = 1,\ldots,n_p$. The values of the resulting bounds $[x_j^-, x_j^+]$ for each random variable X_j, for $j = 1,\ldots,n_p$, are then defined by the quantiles $x_j^- = \mathcal{F}_{X_j(p_j^-)}^{-1}(\alpha_{X_j})$ and $x_j^+ = \mathcal{F}_{X_j(p_j^+)}^{-1}(1-\alpha_{X_j})$. $\mathcal{F}_{X_j(p_j^-)}$ and $\mathcal{F}_{X_j(p_j^+)}$ are the CDF of X_j at the lower and upper bounds p_j^- and p_j^+, respectively. Finally, the confidence region for the random vector $\mathbb{X}$ is

$$\mathbb{X} = \bigtimes_{j=1}^{n_p} [x_j^-, x_j^+] \tag{9}$$

Similarly, the confidence region of the random vector $\boldsymbol{Z}$ can be defined by the probability α_{Z_k} of sampling outside the definition area. The lower and upper bounds of $\boldsymbol{Z}$ are defined around the mean value, such that $z_k^- = \mathcal{F}_{Z_k}^{-1}(\alpha_{Z_k})$ and $z_k^+ = \mathcal{F}_{Z_k}^{-1}(1-\alpha_{Z_k})$. The resulting confidence region for $\boldsymbol{Z}$ is

$$\mathbb{Z} = \bigtimes_{k=1}^{n_z} [z_k^-, z_k^+] \tag{10}$$

The domain of definition to build the surrogate models of the constraint functions $g_i(\cdot)$ is finally defined as the Cartesian product of the marginal confidence regions of each variable $\mathbb{S} = \mathbb{D} \times \mathbb{X} \times \mathbb{Z}$. Using this domain of definition allows us to save and reuse the dataset enriched during the DO and the RA stages at each iteration of SORA.

B. Multifidelity Bayesian Optimization

In this section, for the sake of simplicity in presenting the multifidelity and Bayesian optimization frameworks, a generic function f that takes $\boldsymbol{x}$ as inputs and provides y as output is considered:

$$f : \mathcal{X} \in \mathbb{R}^d \to \mathbb{R}$$
$$\boldsymbol{x} \to y = f(\boldsymbol{x})$$

1. Autoregressive Models

Several multifidelity modeling techniques using GPs are documented in the literature [31–33]. One of the most popular techniques

is the autoregressive model (AR1) [32]. It is based on the assumption that two consecutive fidelity levels follow a linear dependency. In the present work, for the sake of simplicity, the AR1 method is favored for the construction of multifidelity Bayesian optimization in SORA. Yet, other multifidelity modeling techniques may be used, depending on the relationship between the different fidelity levels [34].

The multifidelity aspect is induced by the presence of L numerical codes $\{f_\ell(\cdot)\}_{\ell=1,\dots,L}$ of different levels of fidelity $\ell \in \{1,\dots,L\}$. Note that $f_1(\cdot)$ is the cheapest and lowest fidelity level, and $f_L(\cdot)$ is the most computationally expensive model with the highest fidelity level. For each fidelity level ℓ, a DoE $\mathcal{D}_\ell = \{\mathcal{X}_\ell, \mathcal{Y}_\ell\}$ of size M_ℓ is considered, with $\mathcal{X}_\ell = \{\boldsymbol{x}_\ell^1,\dots,\boldsymbol{x}_\ell^{M_\ell}\}$ and $\mathcal{Y}_\ell = \{y_\ell^1,\dots,y_\ell^{M_\ell}\}$, where $y_\ell^i = f_\ell(\boldsymbol{x}_\ell^i)$ is the output corresponding to the ith point of the input DoE, and the output DoE vector is defined as $\boldsymbol{y}_\ell = [y_\ell^1,\dots,y_\ell^{M_\ell}]^T$. The surrogate model of f_ℓ is denoted by $F_\ell(\cdot)$. For each $F_\ell(\cdot)$, the prior mean function is assumed to be constant, and a family of covariance functions $k_\ell(\cdot,\cdot)$ is prescribed.

The linear relationship between two successive fidelity levels reads $F_\ell(\cdot) = \rho_{\ell-1}(\cdot)F_{\ell-1}(\cdot) + \gamma_\ell(\cdot)$, where $\gamma_\ell(\cdot)$ is a GP corrector with prior mean μ_{γ_ℓ} and covariance kernel $k_{\gamma_\ell}(\cdot,\cdot)$, independent of $F_{\ell-1}(\cdot)$. Note that $\rho_{\ell-1}(\cdot)$ is a scaling function that represents the linear dependency between the models of levels ℓ and $\ell-1$. This scaling function is often assumed to be a constant parameter $\rho_{\ell-1}(\cdot) = \rho_{\ell-1}$ that is learnt during the GP training [32]. The values of the hyperparameters of the L GPs are determined within a single optimization problem. The lower-fidelity model at level $\ell = 1$ is defined as $F_1(\cdot) = \gamma_1(\cdot)$.

A sequential training process of the GPs is proposed by Le Gratiet and Garnier [55] considering nested DoEs for the different fidelity levels. This recursive construction avoids the resolution of a single and large optimization problem. In this framework, the GP prior $F_{\ell-1}(\cdot)$ for the definition of $F_\ell(\cdot)$ is replaced by its posterior $\hat{F}_{\ell-1}(\cdot)$. At level ℓ, the only hyperparameters that are learned are the scaling factor $\rho_{\ell-1}$ and the hyperparameters of the GP corrector $\gamma_\ell(\cdot)$. Once the training phase is performed, the mean and variance posterior prediction for level $\ell = 1$ are defined as for a standard GP, by the conditional properties of a multivariate Gaussian distribution. The posterior mean $\hat{\mu}_\ell(\cdot)$ and variance $\hat{\sigma}_\ell{}^2(\cdot)$ for each level $\ell \in \{2,\dots,L\}$ read

$$\hat{\mu}_\ell(\boldsymbol{x}) = \rho_{\ell-1}\hat{\mu}_{\ell-1}(\boldsymbol{x}) + \hat{\mu}_{\gamma_\ell} + \boldsymbol{k}_\ell(\boldsymbol{x})^T\boldsymbol{K}_\ell^{-1}(\boldsymbol{y}_\ell - \rho_{\ell-1}\hat{\boldsymbol{\mu}}_{\ell-1}(\mathcal{X}_\ell) - \hat{\mu}_{\gamma_\ell}\boldsymbol{1}) \tag{11}$$

$$\hat{\sigma}_\ell{}^2(\boldsymbol{x}) = \rho_{\ell-1}^2\hat{\sigma}_{\ell-1}{}^2(\boldsymbol{x}) + k_\ell(\boldsymbol{x},\boldsymbol{x}) - \boldsymbol{k}_\ell(\boldsymbol{x})^T\boldsymbol{K}_\ell^{-1}\boldsymbol{k}_\ell(\boldsymbol{x}) \tag{12}$$

where $\boldsymbol{K}_\ell = [k_\ell(\boldsymbol{x}_\ell^i, \boldsymbol{x}_\ell^j)]_{i,j=1,\dots,M_\ell}$ is the block of the covariance matrix corresponding to the DoE $\mathcal{D}_\ell$ at level ℓ. Note that $\boldsymbol{k}_\ell(\boldsymbol{x}) = [k_\ell(\boldsymbol{x}, \boldsymbol{x}_\ell^i)]_{i=1,\dots,M_\ell}$ and $\hat{\mu}_{\gamma_\ell}$ is the posterior mean of $\gamma_\ell(\cdot)$. In the presence of noisy observations (e.g., nondeterministic observations), it is also possible to add a Gaussian noise of variance (also called nugget) σ_ℓ^2 to the diagonal of the matrix $\boldsymbol{K}_\ell$, such as $\hat{\boldsymbol{K}}_\ell = \boldsymbol{K}_\ell + \sigma_\ell^2\boldsymbol{I}$, with $\boldsymbol{I}$ the identity matrix.

According to the framework presented previously, the vector $\boldsymbol{x}$ of this section corresponds to $\{\boldsymbol{d}, \boldsymbol{p}\}$ for the DO phase, and to $\{\boldsymbol{x}, \boldsymbol{z}\}$ for the RA phase. With the work in the augmented space for the surrogate model of each constraint, the vector $\boldsymbol{x}$ corresponds to $\{\boldsymbol{d}, \boldsymbol{x}, \boldsymbol{z}\}$. The input variables of the problem (design and uncertain) are assumed to be independent. A classical approach is used to define multivariate kernels, as a product of single variable kernel (such as Matern and squared exponential).

2. Bayesian Optimization (BO)

BO approaches based on active learning strategies [56] involve surrogate models for the objective function and for each constraint function. The surrogate models are built from a limited database and then enriched with additional evaluations of the exact simulators in areas of interest along the optimization process.

A constrained optimization problem is classically formulated as

$$\min_{\boldsymbol{x}\in\mathbb{X}} f(\boldsymbol{x}) \qquad \text{s.t.} \quad g(\boldsymbol{x}) \leqslant 0 \tag{13}$$

where $f(\cdot)$ is the objective function and $g(\cdot)$ is the considered constraint function. Each function depends on $\boldsymbol{x}$ defined on a set $\mathbb{X}$.

The selection process of the new evaluation points to enrich the surrogate models and find the global optimum is called active learning. It is achieved through the resolution of an auxiliary optimization problem involving an acquisition function (also named as infill criterion). For unconstrained optimization problems, several acquisition functions are reported in the literature. Popular examples are the *probability of improvement* (PI) [57,58], the *expected improvement* (EI) [56], and the *lower confidence bound* (LCB) [59,60]. The new point $\boldsymbol{x}^{\text{new}}$ is selected by optimizing (minimizing or maximizing) one of these criteria, then $f(\boldsymbol{x}^{\text{new}})$ is evaluated and the current DoE is enriched.

In the present paper, the LCB function is used to target the global optimum of $f(\cdot)$ [61]. This function is more convenient than EI to define a convergence criterion in order to stop the BO algorithms in RA and DO at each iteration of SORA. LCB provides the solution of the optimization problem, based on the mean GP prediction $\hat{\mu}_f(\cdot)$ and its associated variance prediction $\hat{\sigma}_f^2(\cdot)$ (similarly defined to Eqs. (11) and (12) but for single fidelity GP). The LCB function is defined as

$$\text{LCB}(\boldsymbol{x}) = \hat{\mu}_f(\boldsymbol{x}) - \alpha\hat{\sigma}_f(\boldsymbol{x}) \tag{14}$$

where α is a positive scalar parameter describing the exploitation/exploration balance. Large value of α tend to prioritize exploration.

Several infill criteria for constraints handling have also been proposed, for instance, the *probability of feasibility* [62] or the *expected violation* (EV) [63]. The EV function quantifies the violation of the constraint $g(\cdot)$ at $\boldsymbol{x}$ based on the GP mean prediction $\hat{\mu}_g(\cdot)$ and its associated variance $\hat{\sigma}_g^2(\cdot)$. It reads

$$\text{EV}(\boldsymbol{x}) = \hat{\mu}_g(\boldsymbol{x})\Phi\left(\frac{\hat{\mu}_g(\boldsymbol{x})}{\hat{\sigma}_g(\boldsymbol{x})}\right) + \hat{\sigma}_g(\boldsymbol{x})\phi\left(\frac{\hat{\mu}_g(\boldsymbol{x})}{\hat{\sigma}_g(\boldsymbol{x})}\right) \tag{15}$$

where $\Phi(\cdot)$ and $\phi(\cdot)$, respectively, denote the CDF and the PDF of the normal distribution. The new point $\boldsymbol{x}^{\text{new}}$ is selected such that

$$\boldsymbol{x}^{\text{new}} = \underset{\boldsymbol{x}\in\mathcal{X}}{\text{argmin}}\ \text{LCB}(\boldsymbol{x}) \qquad \text{s.t.} \quad \text{EV}(\boldsymbol{x}) \leqslant T \tag{16}$$

where T is a threshold corresponding to the maximum accepted constraint violation.

3. Multifidelity Bayesian Optimization (MFBO)

BO acquisition functions must be adapted to the multifidelity framework in order to select the location of the new evaluation point as well as the fidelity level for this evaluation. This selection is implemented either as a coupled procedure or a sequential procedure as reported in the literature [64–69]. A sequential procedure is implemented in this paper as described in [36].

Let $\text{LCB}(\ell, \boldsymbol{x})$ and $\text{EV}(\ell, \boldsymbol{x})$ denote the LCB and EV functions computed at $\boldsymbol{x}$ with the GP predictions at level ℓ. First, $\boldsymbol{x}^{\text{new}}$ is identified from Eq. (16) with the LCB function using the prediction of posterior mean and variance corresponding to the higher fidelity GP. Then, the level of fidelity ℓ^{new} is identified. Meliani et al. [36] proposed a criterion based on the variance reduction $\sigma^2_{\text{red}}(\ell, \boldsymbol{x}^{\text{new}})$, associated with the addition of $\boldsymbol{x}^{\text{new}}$ at level ℓ in the DoE and weighted by the associated computational cost. The variance reduction reads

$$\sigma^2_{\text{red}}(\ell, \boldsymbol{x}^{\text{new}}) = \sum_{i=1}^{\ell}\hat{\sigma}^2_{\gamma,i}(\boldsymbol{x}^{\text{new}})\prod_{j=i}^{\ell-1}\rho_j^2 \tag{17}$$

Note that $\hat{\sigma}^2_{\gamma,i}$ is the posterior variance of the GP corrector at fidelity i, and ρ_j the scaling factor in the AR1 formulation; $\{\boldsymbol{x}^{\text{new}}, \ell^{\text{new}}\}$ are defined as

$$\begin{cases} \boldsymbol{x}^{\text{new}} = \underset{\boldsymbol{x}\in\mathcal{X}}{\text{argmin}}\ \text{LCB}(L,\boldsymbol{x}) \quad \text{s.t.} \quad \text{EV}(L,\boldsymbol{x}) \leqslant T \\ \ell^{\text{new}} = \underset{\ell\in\{1,\ldots,L\}}{\text{argmax}}\ \frac{\sigma^2_{\text{red}}(\ell,\boldsymbol{x}^{\text{new}})}{\text{cost}_{\text{total}}(\ell)^2} \end{cases} \tag{18}$$

As AR1 is used to construct the multifidelity surrogate models, a nested structure of the DoEs is considered. Thus, if a data point is added at level ℓ, it is also added at all lower fidelity levels. The corresponding computational cost associated with an evaluation at level ℓ is therefore $\text{cost}_{\text{total}}(\ell) = \sum_{i=1}^{\ell} c_i$, with c_i the computational cost of the numerical solver used at level i. The enrichment of the surrogate model stops when two successively selected points are sufficiently close (i.e., whose distance is less than 10^{-3} in the normalized space). If this stopping criterion is not reached, a stagnation criterion on the value of the objective function at the enrichment point is used (here over 10 successive iterations).

It can be noted that the enrichment criterion used to manage fidelity selection is weighted by the square of the computational cost. Other criteria use simply the cost to penalize the reduction of variance (e.g., in [70]). As explained in [36], the authors compared these two penalization criteria (with simply the cost and with the square of the cost) on different cases and concluded that considering the square of the cost to weight the fidelity selection criterion was the most efficient strategy. An explanation given in [36] is that it is reasonable to consider the square of the cost, as the variance of the level ℓ scales with the square of $\rho_{\ell-1}$ in Eq. (12), corresponding to the correlation between the levels ℓ and $\ell-1$, directly linked to the quantity of information shared between these levels.

III. Multifidelity Bayesian Sequential Optimization and Reliability Assessment (MFB-SORA)

A. General Framework

The MFB-SORA algorithm is derived from SORA, which formulates the RBDO problem as a sequence of DO [Eq. (3)] and RA [Eq. (4)]. These optimization problems are solved using multifidelity surrogate models which are enriched along the SORA process. The construction of the surrogate models for the constraint functions $g_i(\cdot)$ is carried out in the augmented space to reuse information from DO and RA along the iterations of SORA.

In the following, two levels of fidelity named low-fidelity (LF) and high-fidelity (HF) are considered for the sake of simplicity, without loss of generality. Since the AR1 multifidelity model (Sec. II.B.1) and the multifidelity infill criterion (Sec. II.B.3) are presented for L levels of fidelity, the proposed approach is generalizable to more than two levels of fidelity, and independent of the number of available levels of fidelity. For example, GP-based multifidelity techniques have been applied in [71] with more than two levels of fidelity. The MFB-SORA workflow is presented in Fig. 3 and the corresponding algorithm is given in Algorithm 1. The

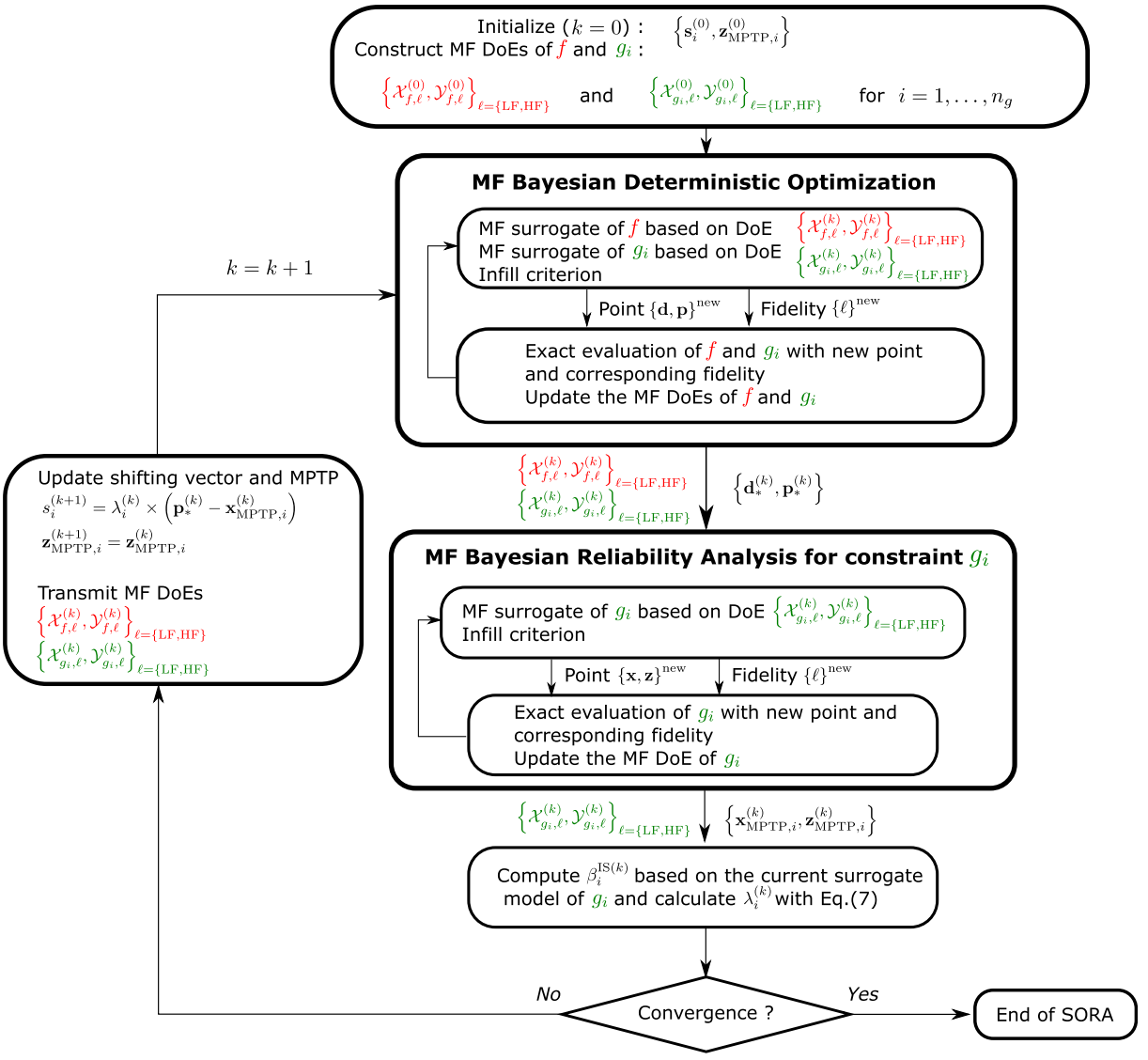

Fig. 3 Workflow of MFB-SORA for two levels of fidelity (LF and HF). DoEs for objective and constraint functions are, respectively, indicated in red and green.

Algorithm 1: MFB-SORA algorithm for two levels of fidelity (LF and HF).

$k \leftarrow 0$ ▷ SORA loop counter
$\boldsymbol{s}_{i,\text{corr}}^{(k)} \leftarrow \boldsymbol{0}$, for $i = 1, \ldots, n_g$
$\boldsymbol{z}_{\text{MPTP},i}^{(k)} \leftarrow \boldsymbol{\mu}_Z$, for $i = 1, \ldots, n_g$
$\{\mathcal{X}_{f,\ell}^{(k)}, \mathcal{Y}_{f,\ell}^{(k)}\}_{\ell=\{\text{LF,HF}\}}$
$\{\mathcal{X}_{g_i,\ell}^{(k)}, \mathcal{Y}_{g_i,\ell}^{(k)}\}_{\ell=\{\text{LF,HF}\}}$ (for $i = 1, \ldots, n_g$)
while (stopping criterion not reached) **do**
  DO phase
  $\{\boldsymbol{d}_*^{(k)}, \boldsymbol{p}_*^{(k)}\}$ and $\{\mathcal{X}_{f,\ell}^{(k)}, \mathcal{Y}_{f,\ell}^{(k)}, \mathcal{X}_{g_i,\ell}^{(k)}, \mathcal{Y}_{g_i,\ell}^{(k)}\}_{\ell=\{\text{LF,HF}\}} \leftarrow$ Solve Eq. (3) ▷ See Algorithm 2
  RA phase
  for $i = 1, \ldots, n_g$ **do**
    $\{\boldsymbol{x}_{\text{MPTP},i}^{(k)}, \boldsymbol{z}_{\text{MPTP},i}^{(k)}\}$ and $\{\mathcal{X}_{g_i,\ell}^{(k)}, \mathcal{Y}_{g_i,\ell}^{(k)}\}_{\ell=\{\text{LF,HF}\}} \leftarrow$ Solve Eq. (4) ▷ See Algorithm 3
    $\boldsymbol{s}_i^{(k+1)} \leftarrow \boldsymbol{p}_*^{(k)} - \boldsymbol{x}_{\text{MPTP},i}^{(k)}$
    $\lambda_i^{(k)} \leftarrow \beta_i^t / \beta_i^{\text{IS}(k)}$
    $\boldsymbol{s}_{i,\text{corr}}^{(k+1)} \leftarrow \lambda_i^{(k)} \boldsymbol{s}_i^{(k+1)}$
  end for
  $k \leftarrow k + 1$
end while

Algorithm 2: Multifidelity BO for DO for two levels of fidelity (LF and HF)

Require: $\{\mathcal{X}_{f,\ell}^{(k)}, \mathcal{Y}_{f,\ell}^{(k)}, \mathcal{X}_{g_i,\ell}^{(k)}, \mathcal{Y}_{g_i,\ell}^{(k)}\}_{\ell=\{\text{LF,HF}\}}$ and $\{\boldsymbol{s}_{i,corr}^{(k)}, \boldsymbol{z}_{\text{MPTP},i}^{(k)}\}$ (for $i = 1, \ldots, n_g$)
Ensure: $\{\boldsymbol{d}_*^{(k)}, \boldsymbol{p}_*^{(k)}\}$ and $\{\mathcal{X}_{f,\ell}^{(k)}, \mathcal{Y}_{f,\ell}^{(k)}, \mathcal{X}_{g_i,\ell}^{(k)}, \mathcal{Y}_{g_i,\ell}^{(k)}\}_{\ell=\{\text{LF,HF}\}}$ updated
  while (stopping criterion not reached) **do**
    Construct multifidelity surrogate models of $f(\cdot)$ and $g_i(\cdot)$ with current DoEs
    $\boldsymbol{q}_{\text{DO}}^{\text{new}} \leftarrow$ Solve Eq. (19)
    $\ell_{\text{DO}}^{\text{new}} \leftarrow$ Solve Eq. (20)
    $\mathcal{X}_{f,\text{LF}}^{(k)} \leftarrow \mathcal{X}_{f,\text{LF}}^{(k)} \cup \{\boldsymbol{q}_{\text{DO}}^{\text{new}}\}$ and $\mathcal{Y}_{f,\text{LF}}^{(k)} \leftarrow \mathcal{Y}_{f,\text{LF}}^{(k)} \cup \{f^{LF}(\boldsymbol{q}_{\text{DO}}^{\text{new}})\}$
    $\mathcal{X}_{g_i,\text{LF}}^{(k)} \leftarrow \mathcal{X}_{g_i,\text{LF}}^{(k)} \cup \{\boldsymbol{q}_{\text{DO,AS}}^{\text{new}}\}$ and $\mathcal{Y}_{g_i,\text{LF}}^{(k)} \leftarrow \mathcal{Y}_{g_i,\text{LF}}^{(k)} \cup \{g_i^{LF}(\boldsymbol{q}_{\text{DO,AS}}^{\text{new}})\}$ (for $i = 1, \ldots, n_g$)
    if $\ell_{\text{DO}}^{\text{new}} =$'HF' **then**
      $\mathcal{X}_{f,\text{HF}}^{(k)} \leftarrow \mathcal{X}_{f,\text{HF}}^{(k)} \cup \{\boldsymbol{q}_{\text{DO}}^{\text{new}}\}$ and $\mathcal{Y}_{f,\text{HF}}^{(k)} \leftarrow \mathcal{Y}_{f,\text{HF}}^{(k)} \cup \{f^{HF}(\boldsymbol{q}_{\text{DO}}^{\text{new}})\}$
      $\mathcal{X}_{g_i,\text{HF}}^{(k)} \leftarrow \mathcal{X}_{g_i,\text{HF}}^{(k)} \cup \{\boldsymbol{q}_{\text{DO,AS}}^{\text{new}}\}$ and $\mathcal{Y}_{g_i,\text{HF}}^{(k)} \leftarrow \mathcal{Y}_{g_i,\text{HF}}^{(k)} \cup \{g_i^{\text{HF}}(\boldsymbol{q}_{\text{DO,AS}}^{\text{new}})\}$ (for $i = 1, \ldots, n_g$)
    end if
    Update the surrogate models of $f(\cdot)$ and $g_i(\cdot)$ for $i = 1, \ldots, n_g$
  end while

multifidelity DoEs for the objective function $f(\cdot)$ and constraint functions $g_i(\cdot)$ at fidelity level ℓ, at SORA iteration k, are denoted, respectively, by $\{\mathcal{X}_{f,\ell}^{(k)}, \mathcal{Y}_{f,\ell}^{(k)}\}$ and $\{\mathcal{X}_{g_i,\ell}^{(k)}, \mathcal{Y}_{g_i,\ell}^{(k)}\}$.

As discussed in Sec. II.B.1, in order to use a sequential training in AR1, the multifidelity DoEs must be nested. Therefore, when a data point is added to a high-fidelity DoE, it should also be added to lower-fidelity DoEs. During each DO cycle, the multifidelity DoEs of $f(\cdot)$ and $g_i(\cdot)$, $i = 1, \ldots, n_g$ are enriched at the same points in the augmented space. The surrogate model for each constraint is further enriched in the RA phase. During the DO phase, the DoE of each constraint is enriched according to the design variables, modified by the corrected shifting vector $\boldsymbol{s}_{i,\text{corr}}^{(k)}$, with the uncertain variables $\boldsymbol{Z}$ fixed at $\boldsymbol{z}_{\text{MPTP},i}^{(k)}$. During the RA phase, the DoE of each constraint is enriched according to the uncertain variables, with the design variables $\boldsymbol{d}$ and $\boldsymbol{p}$ fixed at $\boldsymbol{d}_*^{(k)}$ and $\boldsymbol{p}_*^{(k)}$. Enrichment strategies are presented in Secs. III.B and III.C. Different stopping criteria for the SORA process are available. In the present implementation, the stopping criterion is based on the distance between the deterministic optimal solutions given by the DO phase for two consecutive iterations of SORA.

When the linear assumption between the different levels of fidelity no longer holds, alternative multifidelity approaches should be favored, such as the nonlinear autoregressive multifidelity Gaussian process (NARGP) [33]. Comparison of various multifidelity surrogate strategies are discussed in [34].

B. Multifidelity Bayesian Optimization for Deterministic Optimization

The DO step in SORA is solved as an optimization subproblem [Eq. (3)]. The workflow for two fidelity levels is presented in Algorithm 2. For the first SORA iteration, a limited size multifidelity DoE is generated. During the following iterations, the enrichment is performed using the LCB acquisition function for the objective function and the EV function for the constraints handling:

$$\begin{aligned} \boldsymbol{q}_{\text{DO}}^{\text{new}} &= \underset{\boldsymbol{q}}{\text{argmin}}\ \text{LCB}_f(L, \boldsymbol{q}) \\ \text{s.t.}\quad & \text{EV}_{g_i}(L, \boldsymbol{q}_{\text{shifted}}) \leq T_i \quad \text{for } i = 1, \ldots, n_g \end{aligned} \tag{19}$$

where $\boldsymbol{q} = [\boldsymbol{d}, \boldsymbol{p}]^T$ is the design vector. $\text{LCB}_f(L, \boldsymbol{q})$ is the LCB computed with the high-fidelity GP prediction of $f(\cdot)$ at $\boldsymbol{q}$. $\text{EV}_{g_i}(L, \boldsymbol{q}_{\text{shifted}})$ is the EV computed with the high-fidelity GP prediction of $g_i(\cdot)$ at $\boldsymbol{q}_{\text{shifted}} = [\boldsymbol{d}, \boldsymbol{p} - \boldsymbol{s}_{i,\text{corr}}^{(k)}]^T$. Note that $\boldsymbol{q}_{\text{DO,AS}}^{\text{new}} = [\boldsymbol{d}_*^{(k)}, \boldsymbol{p}_*^{(k)} - \boldsymbol{s}_{i,\text{corr}}^{(k)}, \boldsymbol{z}_{\text{MPTP},i}^{(k)}]_{\text{DO}}^{\text{new}^T}$ denotes the shifted point in the augmented space corresponding to $\boldsymbol{q}_{\text{DO}}^{\text{new}}$.

The selected fidelity level is such that

$$\ell_{\text{DO}}^{\text{new}} = \underset{\ell \in \{1, \ldots, L\}}{\text{argmax}} \frac{\sigma_{\text{red},f}^2(\ell, \boldsymbol{q}_{\text{DO}}^{\text{new}})}{\text{cost}_{\text{total}}(\ell)^2} \tag{20}$$

where $\sigma_{\text{red},f}^2(\ell, \cdot)$ denotes the variance reduction of the surrogate model of $f(\cdot)$ when evaluated at the location $\boldsymbol{q}_{\text{DO}}^{\text{new}}$ with the fidelity level ℓ. The $\text{cost}_{\text{total}}(\ell)$ is the total computational cost associated with the evaluation of the exact solver at the fidelity level ℓ and the lower level fidelity solvers to respect the nested DoE property.

C. Multifidelity Bayesian Optimization for Reliability Assessment

The RA step in SORA is solved using a multifidelity Bayesian optimization subproblem. The workflow for two levels of fidelity is presented in Algorithm 3, without loss of generality. For each $g_i(\cdot)$, $i = 1, \ldots, n_g$, working in the augmented space allows us to reuse the previous multifidelity DoEs $\{\mathcal{X}_{g_i,\ell}^{(k)}, \mathcal{Y}_{g_i,\ell}^{(k)}\}_{\ell=\{\text{LF,HF}\}}$. For each constraint $g_i(\cdot)$, the corresponding surrogate model is then enriched independently from the subdomain of the augmented space defined by the solution $\boldsymbol{d}_*^{(k)}$ of the previous DO.

Algorithm 3: Multifidelity BO for RA for the constraint $g_i(\cdot)$ for two levels of fidelity (LF and HF)

Require: $\{\mathcal{X}_{g_i,\ell}^{(k)}, \mathcal{Y}_{g_i,\ell}^{(k)}\}_{\ell=\{\text{LF,HF}\}}$ and $\{\boldsymbol{d}_*^{(k)}, \boldsymbol{p}_*^{(k)}\}$
Ensure: $\{\boldsymbol{x}_{\text{MPTP},i}^{(k)}, \boldsymbol{z}_{\text{MPTP},i}^{(k)}\}$ and $\{\mathcal{X}_{g_i,\ell}^{(k)}, \mathcal{Y}_{g_i,\ell}^{(k)}\}_{\ell=\{\text{LF,HF}\}}$ updated
  while (stopping criterion not reached) **do**
    Construct surrogate of $g_i(\cdot)$
    $\boldsymbol{w}_{\text{RA}}^{\text{new}} \leftarrow$ Solve Eq. (22)
    $\ell_{\text{RA}}^{\text{new}} \leftarrow$ Solve Eq. (23)
    $\mathcal{X}_{g_i,\text{LF}}^{(k)} \leftarrow \mathcal{X}_{g_i,\text{LF}}^{(k)} \cup \{\boldsymbol{w}_{\text{RA,AS}}^{\text{new}}\}$ and $\mathcal{Y}_{g_i,\text{LF}}^{(k)} \leftarrow \mathcal{Y}_{g_i,\text{LF}}^{(k)} \cup \{g_i^{\text{LF}}(\boldsymbol{w}_{\text{RA,AS}}^{\text{new}})\}$
    if $\ell_{\text{RA}}^{\text{new}} =$'HF' **then**
      $\mathcal{X}_{g_i,\text{HF}}^{(k)} \leftarrow \mathcal{X}_{g_i,\text{HF}}^{(k)} \cup \{\boldsymbol{w}_{\text{RA,AS}}^{\text{new}}\}$ and
      $\mathcal{Y}_{g_i,\text{HF}}^{(k)} \leftarrow \mathcal{Y}_{g_i,\text{HF}}^{(k)} \cup \{g_i^{\text{HF}}(\boldsymbol{w}_{\text{RA,AS}}^{\text{new}})\}$
    end if
    Update the surrogate model of $g_i(\cdot)$
  end while

The RA problem in Eq. (4) is solved in the standard space defined by an isoprobabilistic transformation, related to the joint PDF of $\boldsymbol{X}$ and $\boldsymbol{Z}$, with $\boldsymbol{X}$ parameterized by $\boldsymbol{p}_*^{(k)}$. For the sake of simplicity, Eq. (4) is reformulated as follows:

$$\min_{\boldsymbol{w}} g_i(\boldsymbol{d}_*^{(k)}, \boldsymbol{w}) \quad \text{s.t.} \quad \|\mathcal{T}_{\boldsymbol{p}_*^{(k)}}(\boldsymbol{w})\| = \beta_i^t \tag{21}$$

where $\boldsymbol{w} = [\boldsymbol{X}, \boldsymbol{Z}]^T$ is the random vector in the physical space.

Similarly to DO, Eq. (21) is solved by multifidelity BO for each constraint $g_i(\cdot)$. The DoE is enriched with active learning by new data points $\boldsymbol{w}_{\text{RA}}^{\text{new}}$ such that

$$\boldsymbol{w}_{\text{RA}}^{\text{new}} = \underset{\boldsymbol{w}}{\text{argmin}}\, \text{LCB}_{g_i}(L, \boldsymbol{w}) \quad \text{s.t.} \quad \|\mathcal{T}_{\boldsymbol{p}_*^{(k)}}(\boldsymbol{w})\| = \beta_i^t \tag{22}$$

where $\text{LCB}_{g_i}(L, \boldsymbol{w})$ is the LCB computed with the high-fidelity GP prediction of $g_i(\cdot)$ at $\boldsymbol{w}$. The level of fidelity is then selected following Eq. (18):

$$\ell_{\text{RA}}^{\text{new}} = \underset{\ell \in \{1,\ldots,L\}}{\text{argmax}} \frac{\sigma^2_{\text{red},g_i}(\ell, \boldsymbol{w}_{\text{RA}}^{\text{new}})}{\text{cost}_{\text{total}}(\ell)^2} \tag{23}$$

where $\sigma^2_{\text{red},g_i}(\ell, \cdot)$ is the reduction of variance for the GP of $g_i(\cdot)$. The function $\text{cost}_{\text{total}}(\ell)$ corresponds to the total cost associated with the evaluation of the exact solver at the new point $\boldsymbol{w}_{\text{RA}}^{\text{new}}$ with the selected level of fidelity ℓ and the exact solvers at the lower fidelities.

Note that $\boldsymbol{w}_{\text{RA,AS}}^{\text{new}} = [\boldsymbol{d}_*^{(k)}, \boldsymbol{X}, \boldsymbol{Z}]_{\text{RA}}^{\text{new}^T}$ denotes the point in the augmented space that corresponds to $\boldsymbol{w}_{\text{RA}}^{\text{new}}$.

IV. Computational Experiments

The proposed methodology is applied in this section on five different test cases and compared in terms of computational performance and accuracy with different classical RBDO techniques: SORA (two versions with and without IS-based correcting factor) and a two-level approach to have a reference solution. The first test case is a simple analytical case for illustration purposes. The second case deals with the optimization of a vehicle brake disk [42,45] where analytical functions are involved. The third RBDO problem involves an aerospace speed reducer physical case [46,47] described through analytical functions. Finally, two representative aerospace optimization problems are considered: a solid-propellant rocket booster RBDO problem and a design problem of a sounding rocket. The objective of the numerical experiments is to prove the robustness and efficiency of the proposed multifidelity Bayesian SORA approach (MFB-SORA) regarding cases with different complexity and number of design parameters. To precisely evaluate the performance of each proposed modification of SORA (version with IS), a systematic approach is employed. Consequently, a comprehensive comparison is carried out by incrementally assessing the impact of each modification.

The first evaluated approach deals with the integration of BO for solving the optimization subproblems of SORA. The corresponding method is denoted by B-SORA in the following. The domain of definition for constructing the single fidelity surrogate model of the objective function remains the same along the SORA iterations. Therefore, an initial DoE $\{\mathcal{X}_f, \mathcal{Y}_f\}$ is used for the objective function and enriched during the SORA process. For each of the constraint functions, the domain of definition changes at each step of SORA, and therefore between each DO and RA step. For each specific step, a new surrogate model is constructed from a new DoE, i.e., $\{\mathcal{X}_{g_i}^{\text{DO}}, \mathcal{Y}_{g_i}^{\text{DO}}\}_{i=1,\ldots,n_g}$ for the DO phase and $\{\mathcal{X}_{g_i}^{\text{RA}}, \mathcal{Y}_{g_i}^{\text{RA}}\}_{i=1,\ldots,n_g}$ for the RA phase.

The second evaluated approach deals with the use of the augmented space for the surrogate models of the constraint functions $g_i(\cdot)$. The corresponding method is denoted by B-SORA AS. Similarly to B-SORA, for the objective function, a DoE $\{\mathcal{X}_f, \mathcal{Y}_f\}$ is generated in the design space and then enriched during the steps of SORA. For each constraint function $g_i(\cdot)$, a DoE $\{\mathcal{X}_{g_i}, \mathcal{Y}_{g_i}\}$ is constructed at the beginning of SORA in the augmented space, and then enriched in this augmented space at each step of SORA. The enrichment is performed according to the design variables during DO (with $\boldsymbol{Z}$ fixed), and according to the random variables during RA (with $\boldsymbol{d}$ fixed to the optimal solution of the DO problem).

Finally, the last evaluated approach takes advantage of multiple sources of information to construct multifidelity surrogate models in the augmented space. The optimization subproblems are then solved by multifidelity BO. It is the overall proposed approach in this paper, denoted by MFB-SORA. The multifidelity DoE for the objective function $\{\mathcal{X}_{f,\text{LF}}, \mathcal{X}_{f,\text{HF}}, \mathcal{Y}_{f,\text{LF}}, \mathcal{Y}_{f,\text{HF}}\}$ is constructed in the design variable space at the same locations for all levels of fidelity, with an LHS sampling technique. The multifidelity DoEs of the constraint functions $\{\mathcal{X}_{g_i,\text{LF}}, \mathcal{X}_{g_i,\text{HF}}, \mathcal{Y}_{g_i,\text{LF}}, \mathcal{Y}_{g_i,\text{HF}}\}$, for $i = 1,\ldots,n_g$, are constructed in the augmented space. During the multifidelity BOs, a point added in a given fidelity is automatically added to the lower-fidelity levels.

These three extended versions of SORA (B-SORA, B-SORA AS, and MFB-SORA) are tested on the five test cases. They are compared with the classical SORA technique, the SORA-IS method (involving the correction of the shifting vector through IS), as well as with a two-level approach using Monte Carlo sampling to perform RA. It should be noted that the implementation of the two-level approach was not possible for the two aerospace test cases due to computational cost. For each method and each test case, 50 repetitions are performed with 50 different initial DoEs generated with LHS, in the purpose of evaluating the robustness of the convergence with respect to the initial DoE. The proposed methods are compared in terms of computational cost and precision of the optimal solution noted $\boldsymbol{q}_{\text{opt}}$. For all these test cases, it is considered that each low-fidelity model (objective and constraints) is 10 times cheaper in terms of computational cost than the high-fidelity model, i.e., $c_{\text{LF}} = 0.1$ and $c_{\text{HF}} = 1$. For the three analytical cases, this cost ratio is an assumption. This parameter is fixed, but it is clear that other choices of cost ratio would give different results in terms of the number of evaluations of high-fidelity and low-fidelity codes. This influence is not studied in this article. For the two aerospace optimization cases, this computational cost ratio is also equal to 10, and it has been calculated from the execution times of the high-fidelity and low-fidelity solvers, over several simulations to obtain a consistent average ratio. Computational settings are detailed in Appendix A.

A. Analytical Case

1. Description

The first test case is analytical. It consists of a three-dimensional nonlinear objective function $f(\cdot)$ subjected to two nonlinear probabilistic constraints g_1, g_2 such that

$$\min_{d_0,p_0,p_1} f(d_0, p_0, p_1)$$
$$\text{s.t.} \begin{cases} \mathbb{P}[g_i(d_0, \boldsymbol{X}(p_0, p_1), Z_0) \leqslant 0] \leqslant P_{f,i}^t & \text{for } i = 1,2 \\ -0.5 \leqslant d_0, p_0, p_1 \leqslant 2.5 \end{cases}$$

where d_0, p_0, and p_1 are the deterministic design variables defined in $[-0.5, 2.5]$. $\boldsymbol{X} = [X_0, X_1]^T$ is a random vector of two independent Gaussian variables parameterized by their respective mean p_0 and p_1 such that $X_0 \sim \mathcal{N}(p_0, 0.2)$ and $X_1 \sim \mathcal{N}(p_1, 0.2)$. Z_0 is a random variable such that $Z_0 \sim \mathcal{N}(5, 0.4)$. For each probabilistic constraint $g_i(\cdot)$, the target probability of failure is set to $P_{f,i}^t = 0.01$, for $i = 1,2$. For the objective and each constraint function, two fidelity models (LF and HF) are available. They are, respectively, denoted as $\{f_{\text{LF}}(\cdot), f_{\text{HF}}(\cdot)\}$ and $\{g_{i,\text{LF}}(\cdot), g_{i,\text{HF}}(\cdot)\}_{i=1,2}$. These functions are presented in Appendix A.

2. Results

The results of the 50 repetitions of each technique are summarized in Table 1. These results are presented as a median solution

Table 1 Analytical case: RBDO solution for the two-level, SORA, and SORA-IS strategies and median solution for B-SORA, B-SORA AS, and MFB-SORA computed over 50 repetitions[a]

	$f(\boldsymbol{q}_{\text{opt}})$	$\boldsymbol{q}_{\text{opt}}$			$P_{f,1}$	$P_{f,2}$
Two-level	6.461	[2.5,	0.422,	1.089]	1×10^{-2}	1×10^{-2}
SORA	6.470	[2.5,	0.422,	1.090]	1×10^{-2}	1×10^{-2}
SORA-IS	6.462	[2.5,	0.421,	1.089]	1×10^{-2}	1×10^{-2}
B-SORA	6.472	[2.5,	0.422,	1.090]	9.9×10^{-3}	1×10^{-2}
	(6.4×10^{-4})	(0,	6.8×10^{-5},	6.5×10^{-5})	(1.1×10^{-5})	(3.9×10^{-6})
B-SORA AS	6.471	[2.5,	0.422,	1.090]	9.9×10^{-3}	1×10^{-2}
	(5.2×10^{-4})	(0,	1.9×10^{-4},	1.5×10^{-5})	(2.4×10^{-5})	(8.8×10^{-7})
MFB-SORA	6.471	[2.5,	0.422,	1.090]	9.9×10^{-3}	1×10^{-2}
	(7.1×10^{-4})	$(2.2\times10^{-6}$,	2.1×10^{-4},	3.1×10^{-5})	(2.7×10^{-5})	(2.0×10^{-6})

[a]The first column corresponds to the median of the objective function value $f(\boldsymbol{q}_{\text{opt}})$, and the last columns provide their associated input and constraint values. Median values are indicated, and corresponding interquartile ranges are given in parentheses.

over the 50 repetitions. A measure of the dispersion of these results is provided by the interquartile range (between 75% and 25% quantiles), given in parentheses in Table 1. These quantile values (medians and quartiles) correspond to quantiles on the objective function $f(\boldsymbol{q}_{\text{opt}})$ (in the first column), and their associated input and constraint values are given in the second, third, and fourth columns, respectively. For the two-level, SORA and SORA-IS approaches, not subject to DoE setting, only one value is indicated.

The objective function for the RBDO solutions of B-SORA (blue), B-SORA AS (orange), and MFB-SORA (green) is plotted in Fig. 4 as a function of the computational cost for 50 repetitions of each strategy. The cost is given as the number of equivalent HF model evaluations. For MFB-SORA, the total cost is a weighted sum of LF and HF model evaluations, i.e., $c_{\text{total}} = n_{\text{LF}} \times c_{\text{LF}} + n_{\text{HF}} \times c_{\text{HF}}$. The interquartile range over the 50 repetitions is indicated with error bars. Median values for the computational cost and the optimum are represented, and the bar in both axes represents the variability over the 50 repetitions (interquartile range between 75% and 25% quantiles). For the following applications, the results are presented in the same way as for this case. The upper gray dashed line represents the objective value of the solution of SORA, the darker gray dashed line below represents the SORA-IS solution, and the black dashed line represents the double-loop approach solution.

All methods provide similar optimum $\boldsymbol{q}_{\text{opt}} = [2.5, 0.42, 1.09]$ and corresponding objective function values, as shown in Table 1. For B-SORA, B-SORA AS, and MFB-SORA, the median solutions are feasible with respect to each target probability of failure $P^t_{f,i}$ as

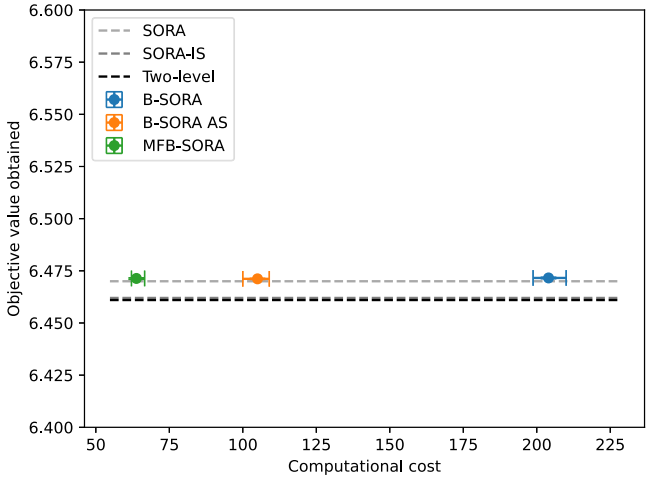

Fig. 4 Analytical case. Objective function evaluated at the RBDO solution as a function of the computational cost for the 50 repetitions of each method.

$P_{f,i} \leqslant P^t_{f,i}$ for $i = 1,2$. It should be noted that all the optimal solutions of the 50 repetitions of each strategy are feasible (not shown here). The dispersion of the solutions in Fig. 4 provided by B-SORA, B-SORA AS, and MFB-SORA is small and of the same order of magnitude, illustrating similar robustness with respect to the initial DoE. As shown in Fig. 4, the values of the optimal objective function obtained by the proposed strategies are closer to the SORA solution than to the ones of SORA-IS and two-level. This can be explained by the fact that the convergence tolerance on $\boldsymbol{q}_{\text{opt}}$ is set to 10^{-3}. If we look at Table 1, the $\boldsymbol{q}_{\text{opt}}$ values are rounded to 10^{-3} and are all equivalent. The results provided by each proposed technique (B-SORA, B-SORA AS, and MFB-SORA) illustrate a progressive improvement of the results with respect to the computational cost, in terms of median and interquartile range values, as shown by the horizontal error bars in Fig. 4. The median of the computational cost decreases as the strategy is more advanced, and the interquartile decreases with the computational cost, meaning that MFB-SORA is precise and efficient.

The computational cost of B-SORA, B-SORA AS, and MFB-SORA is given in Table 2. It is the median value computed over 50 repetitions for each strategy. The associated interquartile range is given in parentheses. The right column indicates the median and interquartile range of the ratio between the cost of each improved SORA strategy (over the 50 repetitions) and the cost of SORA, here taken as the reference.

As expected, the two-level approach is the most expensive one; SORA brings a significant cost reduction that is further reduced with proposed modified SORA strategies. SORA-IS is also expensive, involving a sampling-based correction factor, but it is more efficient than SORA in terms of final objective function value. The use of surrogate models with BO in B-SORA reduces the overall cost by a factor of almost 7. This median cost reduction is doubled when reusing information along the SORA iteration with B-SORA AS: when the surrogates are built in the augmented space, the overall cost is reduced by a factor of 13. Finally, MFB-SORA further reduces the overall cost, with a final median cost reduced by a factor of 22 with respect to SORA. It should also be noted that each proposed modification slightly reduces the dispersion of the cost associated with each strategy with respect to the initial DoE, with an interquartile range reduced from 9 to 4.5.

B. Vehicle Brake Disk Design Case

1. *Description*

This problem deals with a physical case involving the optimization of a brake disk system [42]. This latter is composed of a brake disk and a pair of brake pads. The failure of this system appears when the damping ratio of the vibration is less than the value of -0.01. This consists of an objective function $f(\cdot)$ corresponding to the backplate thickness subjected to one probabilistic constraint g, such that

Table 2 Analytical case: computational cost of SORA, SORA-IS, the two-level approach, B-SORA, B-SORA AS, and MFB-SORA over 50 repetitions for LF and HF model evaluations and total cost[a]

Parameter	LF cost	HF cost	Total cost	Cost reduction (w.r.t. SORA)
Two-level	—	2×10^6	2×10^6	—
SORA	—	1387	1387	—
SORA-IS	—	2×10^4	2×10^4	—
B-SORA	—	**204.0** (9.0)	**204.0** (9.0)	∼**6.8** (0.4)
B-SORA AS	—	**106.0** (9.0)	**106.0** (9.0)	∼**13.3** (1.1)
MFB-SORA	**106.0** (10.0)	**53.0** (4.0)	**63.7** (4.5)	∼**21.8** (1.5)

[a]Median value and associated interquartile range are, respectively, given in bold and in parentheses. The right column indicates the median and interquartile range of the ratio between the cost of each proposed strategy and the cost of SORA.

$$\min_{\mu_{h3}} f(\mu_{h3}) \quad \text{s.t.} \begin{cases} \mathbb{P}[g(\boldsymbol{X}(\boldsymbol{p}), Z_u, Z_p) \leqslant 0] \leqslant P_f^t \\ \boldsymbol{p} = [\mu_{h1}, \mu_{h2}, \mu_{h3}] \\ 14.5 \leqslant \mu_{h1} \leqslant 15.5 \\ 19.5 \leqslant \mu_{h2} \leqslant 20.5 \\ 12 \leqslant \mu_{h3} \leqslant 20 \end{cases}$$

where μ_{h1}, μ_{h2}, and μ_{h3} are the deterministic design variables to optimize, corresponding, respectively, to the mean of the friction material thickness, the disk thickness and the backplate thickness. According to [45], this case involves the use of a 3D finite element model. As presented in [42], this solver can be replaced by a quadratic polynomial response surface to model the damping ratio. This damping ratio depends on five random parameters: the random vector $\boldsymbol{X}$, the random variable Z_u and the random variable Z_p. $\boldsymbol{X} = [X_1, X_2, X_3]^T$ is a random vector of three independent Gaussian variables parameterized by the mean vector $\boldsymbol{p} = [\mu_{h1}, \mu_{h2}, \mu_{h3}]^T$ such that $X_i \sim \mathcal{N}(p_i, \sigma_i)$ with $\sigma_i = 0.9$ mm, for $i = 1, \ldots, 3$. Z_u and Z_p are two random variables such that $Z_u \sim \mathcal{N}(0.35, 0.01)$ and $Z_u \sim \mathcal{N}(0.5, 0.02)$, corresponding, respectively, to the friction coefficient and the brake pressure (MPa). For the probabilistic constraint $g(\cdot)$, the target probability of failure is set to $P_f^t = 1.5 \times 10^{-2}$. For this constraint function, two fidelity models (LF and HF) are available. The LF model of the objective function is proposed in this paper. The models are, respectively, denoted as $\{f_{\text{LF}}(\cdot), f_{\text{HF}}(\cdot)\}$ and $\{g_{\text{LF}}(\cdot), g_{\text{HF}}(\cdot)\}$. All the functions are presented in Appendix A.

2. Results

The results of the 50 repetitions of each technique are summarized in Table 3. These results are presented as a median solution over the 50 repetitions. The information of the dispersion of these results is provided by the interquartile range, given in parentheses in Table 3. These quantile values (medians and quartiles) correspond to quantiles on the objective function $f(\boldsymbol{q}_{\text{opt}})$ (in the first column), and their associated input and constraint values are given in the second, third and fourth columns, respectively. They are compared to the results of the two-level approach and the six GP-based techniques in [42] (the three hybrid GP techniques: RBMO, GP low-fidelity, and GP high-fidelity). The median and interquartile range for $f(\boldsymbol{q}_{\text{opt}})$ for B-SORA (blue), B-SORA AS (orange), and MFB-SORA (green) are plotted in Fig. 5 as a function of the computational cost for 50 repetitions of each strategy. The cost is given as the number of equivalent HF model evaluations. The upper gray dashed line represents the objective value of the solution of SORA, the darker gray dashed line below represents the SORA-IS solution, and the black dashed line represents the double-loop approach solution.

According to Table 3 and Fig. 5, the proposed Bayesian SORA techniques provide similar median results as SORA-IS, allowing us to conclude that there is no precision loss by using surrogate models in the SORA framework. The solution of these techniques are also

Table 3 Vehicle brake disk case: RBDO solution for SORA and SORA-IS strategies, and median solution for B-SORA, B-SORA AS, and MFB-SORA computed over 50 repetitions[a]

Parameter	$f(\boldsymbol{q}_{\text{opt}})$		$\boldsymbol{q}_{\text{opt}}$		P_f
Two-level	17.5450	[15.5000,	19.5000,	17.5450]	1.5×10^{-2}
SORA	17.5073	[15.5000,	19.5000,	17.5073]	1.6×10^{-2}
SORA-IS	17.5369	[15.5000,	19.5000,	17.5369]	1.5×10^{-2}
GP (low-fidelity)	16.0610	[15.5000,	19.5000,	16.0610]	1.1×10^{-1}
GP (high-fidelity)	17.5176	[15.5000,	19.5000,	17.5176]	1.6×10^{-2}
Hybrid GP	17.5938	[15.5000,	19.5000,	17.5938]	1.4×10^{-2}
Hybrid GP	17.4596	[15.5000,	19.5000,	17.4596]	1.7×10^{-2}
Hybrid GP	17.6792	[15.5000,	19.5000,	17.6792]	1.2×10^{-2}
RBMO	17.4284	[15.5000,	19.5000,	17.4284]	1.7×10^{-2}
B-SORA	17.5371	[15.5000,	19.5000,	17.5371]	1.5×10^{-2}
	(3.6×10^{-3})	$(6.0 \times 10^{-10},$	$2.7 \times 10^{-8},$	$3.6 \times 10^{-3})$	(3.1×10^{-4})
B-SORA AS	17.5402	[15.5000,	19.5000,	17.5402]	1.5×10^{-2}
	(5.0×10^{-3})	$(5.6 \times 10^{-7},$	$1.8 \times 10^{-6},$	$5.0 \times 10^{-3})$	(4.8×10^{-4})
MFB-SORA	17.5367	[15.5000,	19.5000,	17.5367]	1.5×10^{-2}
	(9.1×10^{-3})	$(2.9 \times 10^{-7},$	$3.0 \times 10^{-7},$	$9.1 \times 10^{-3})$	(1.3×10^{-4})

[a]The solutions of the two-level approach and the six GP-based techniques are taken from [42] (the three hybrid GP techniques, RBMO, GP low-fidelity, and GP high-fidelity). The first column corresponds to the median of the objective function value $f(\boldsymbol{q}_{\text{opt}})$, and the last columns provide their associated input and constraint values. Median values are indicated and corresponding interquartile ranges are given in parentheses. For comparison purpose, the estimation of the failure probability is performed with a huge Monte Carlo simulation at the final RBDO solution provided by each method.

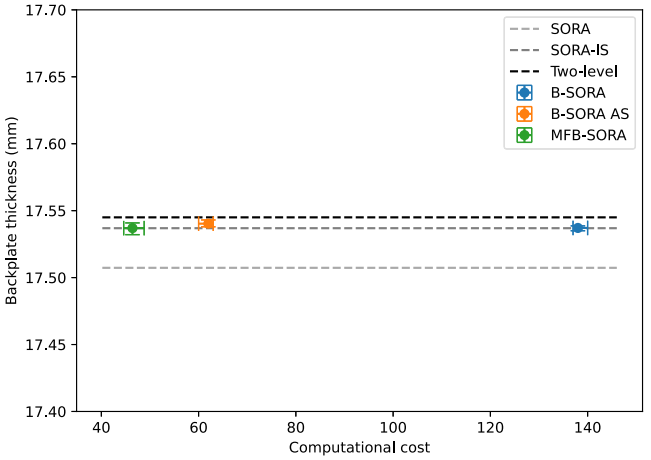

Fig. 5 Vehicle brake disk case. Objective function evaluated at the RBDO solution as a function of the computational cost for the 50 repetitions of each method.

close to the one of the two-level approach, which can be taken as the reference solution. The minimum provided by these SORA-based techniques seems to be lower than the reference solution, with the same level of reliability with respect to the target probability of failure. Indeed, for B-SORA, B-SORA AS, and MFB-SORA, the median solutions are feasible with respect to the target probability of failure P_f^t as $P_f \leqslant P_f^t$, and the interquartile range is sufficiently low to demonstrate the robustness of these techniques. It is interesting to note that the correction of the shifting vector by IS helps SORA to give a solution satisfying the probabilistic constraint, since the solution of classical SORA violates the target probability of failure set to 1.5×10^{-2}. The hybrid GP and RBMO techniques seem to be less robust than the proposed MFB-SORA method, since they provide suboptimal or unfeasible results. As shown in Fig. 5, the results provided by each proposed technique (B-SORA, B-SORA AS, and MFB-SORA) illustrate a progressive improvement in terms of median computational cost, with similar interquartile range values. The proposed MFB-SORA approach is then a robust, accurate, and efficient technique in this test case.

The computational cost of B-SORA, B-SORA AS, and MFB-SORA is given in Table 4. To compare the proposed MFB-SORA approach with the surrogate-based techniques in [42], the costs correspond to the number of constraint function evaluations. It is the median value computed over 50 repetitions for each strategy. The associated interquartile range is given in parentheses. The right column indicates the median and interquartile range of the ratio between the cost of each improved SORA strategy (over the 50 repetitions) and the cost of SORA, here taken as the reference. The total cost of the two-level approach and the six GP-based techniques is the one given in [42] (the three hybrid GP techniques: RBMO, GP low-fidelity, and GP high-fidelity).

As expected, the two-level and the SORA-IS approaches are the most expensive. The SORA framework provides a significant cost reduction with 849 constraint function evaluations. It is clear that the GP-based techniques reduce considerably the total cost. For example, B-SORA is seven times cheaper than SORA. The median cost is further divided by 3 when working in the augmented space with B-SORA-AS. Finally, MFB-SORA further reduces the overall cost, with a final median cost of 31.9 function evaluations (a factor of 26.6 with respect to SORA). This cost is lower than the costs of the five GP-based techniques of [42] involving HF evaluations. It can be considered that the cost of MFB-SORA is nearly the same as the RBMO technique. However, MFB-SORA is robust and accurate in terms of the feasible optimal solution provided, whereas RBMO seems to have difficulties to provide a feasible optimum in this test case. The MFB-SORA is therefore the most efficient and robust technique on the vehicle brake disk presented in this section.

C. Aerospace Speed Reducer Problem

1. *Description*

The third problem is a physical case involving the design optimization of an aircraft speed reducer. This is a classical RBDO problem widely reported in the literature [46,47] for which the objective and constraint functions are analytical. A speed reducer is used in light aircraft to rotate the engine and propeller with efficient speed. The RBDO problem aims at minimizing the mass of the speed reducer while satisfying 11 probabilistic constraints (regarding some quantities such as geometry constraints, bending and contact stress, longitudinal displacement, and stress of the shaft). The problem is formulated as follows:

$$\min_{p_1,\ldots,p_7} f(p_1,\ldots,p_7)$$

$$\text{s.t.} \begin{cases} \mathbb{P}[g_i(X_1(p_1),\ldots,X_7(p_7)) > 0] \leqslant P_{f,i}^t & \text{for } i = 1,\ldots,11 \\ 2.6 \leqslant p_1 \leqslant 3.6 \\ 0.7 \leqslant p_2 \leqslant 0.8 \\ 17 \leqslant p_3 \leqslant 28 \\ 7.3 \leqslant p_4, p_5 \leqslant 8.3 \\ 2.9 \leqslant p_6 \leqslant 3.9 \\ 5 \leqslant p_7 \leqslant 5.5 \end{cases}$$

Table 4 Vehicle brake disk case: computational cost of SORA, SORA-IS, B-SORA, B-SORA AS, and MFB-SORA over 50 repetitions for LF and HF model evaluations and total cost[a]

Parameter	LF cost	HF cost	Total cost	Cost reduction (w.r.t. SORA)
Two-level	—	10^5	10^5	—
SORA	—	849	849	—
SORA-IS	—	10^4	10^4	—
GP (low-fidelity)	132	—	13.2	—
GP (high-fidelity)	—	168	168	—
Hybrid GP	132	30	43.2	—
Hybrid GP	132	40	53.2	—
Hybrid GP	132	50	63.2	—
RBMO	132	22	35.2	—
B-SORA	—	**120.0** (3.0)	**120.0** (3.0)	∼**7.1** (0.2)
B-SORA AS	—	**42.0** (2.0)	**42.0** (2.0)	∼**20.2** (1.0)
MFB-SORA	**40.0** (5.0)	**28.0** (3.0)	**31.9** (3.4)	∼**26.6** (2.8)

[a]The costs of the two-level approach and the six GP-based techniques are taken from [42] (the three Hybrid GP techniques, RBMO, GP low-fidelity and GP high-fidelity). Median value and associated interquartile range are, respectively, given in bold and in parentheses. The right column indicates the median and interquartile range of the ratio between the cost of each proposed strategy and the cost of SORA.

where $\boldsymbol{p} = [p_1, \ldots, p_7]^T$ is the design vector. $\boldsymbol{X} = [X_1, \ldots, X_7]^T$ is a random vector of seven independent Gaussian variables parameterized by $\boldsymbol{p}$ such that $X_i \sim \mathcal{N}(p_i, \sigma_i)$, for $i = 1, \ldots, 7$. The values of $\boldsymbol{\sigma} = [\sigma_1, \ldots, \sigma_7]^T$ are given in Appendix A. These random design variables, respectively, correspond to the gear width X_1, the gear module X_2, the pinion number of teeth X_3, the distance between bearings X_4 and X_5, and the diameter of each shaft X_6 and X_7. The vector $\boldsymbol{\beta}^t = [\beta_1^t, \ldots, \beta_{11}^t]^T$ defines the values of the target reliability indices (RIs), linked to the probabilities of failure $P_{f,i}^t = \Phi(-\beta_i^t)$, where Φ is the CDF of the normal distribution (the values of $\boldsymbol{\beta}^t = [\beta_1^t, \ldots, \beta_{11}^t]^T$ are given in Appendix A).

A multifidelity case of the speed reducer is considered. The LF version of the objective and constraint functions are derived from the HF functions as

$$\boldsymbol{h}_{\mathrm{LF}}(\boldsymbol{x}) = \boldsymbol{\alpha} \times \boldsymbol{h}_{\mathrm{HF}}(\boldsymbol{x}) + \boldsymbol{\eta}$$

where $\boldsymbol{h}_{\mathrm{LF}} = [f_{\mathrm{LF}}(\cdot), g_{1,\mathrm{LF}}(\cdot), \ldots, g_{11,\mathrm{LF}}(\cdot)]^T$ and $\boldsymbol{h}_{\mathrm{HF}} = [f_{\mathrm{HF}}(\cdot), g_{1,\mathrm{HF}}(\cdot), \ldots, g_{11,\mathrm{HF}}(\cdot)]^T$ are, respectively, the vectors of LF and HF functions. Here, a linear relationship between the LF and HF functions is assumed, to be consistent with the choice of the AR1 method. More details on the objective and constraint functions, as well as on settings for vectors $\boldsymbol{\alpha}$ and $\boldsymbol{\eta}$ are given in Appendix A.

2. *Results*

Table 5 presents median solutions and their associated interquartile ranges for $f(\boldsymbol{q}_{\mathrm{opt}})$ (with corresponding input and constraint values over 50 repetitions) for the previously described RBDO strategies. The median and interquartile range for $f(\boldsymbol{q}_{\mathrm{opt}})$ for B-SORA (blue), B-SORA AS (orange), and MFB-SORA (green) are represented in Fig. 6 as a function of the computational cost for 50 repetitions of each strategy. The objective function value of the solution given by SORA from [46] is taken as a reference and represented as a gray dashed line. The darker gray dashed line and the black dashed line represent, respectively, the SORA-IS and the double-loop approach solutions.

All five RBDO methods lead to similar results in terms of optimal design point, around the vector $\boldsymbol{q}_{\mathrm{opt}} = [3.56, 0.7, 17.0, 7.3, 7.747, 3.36, 5.3]$. Similarly to the analytical case, the three enhanced techniques provide a similar small dispersion of the objective function value with respect to the initial DoE (Fig. 6 and Table 5), demonstrating an equivalent robustness. The results provided by each enhanced technique (B-SORA, B-SORA AS, and MFB-SORA) also illustrate a progressive improvement of the results with respect to the computational cost, in terms of median and interquartile range values (Fig. 6).

In the test case definition, the target RI value is either 2 or 3. Table 6 presents the values of the RI at the median optimal solution over the 50 repetitions and its associated interquartile range in parentheses.

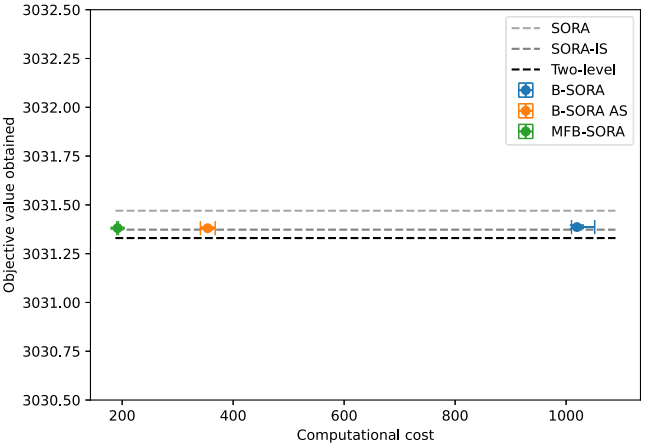

Fig. 6 Speed reducer case. Objective function evaluated at the RBDO solution as a function of the computational cost for the 50 repetitions of each method.

In Table 6, "–" indicates that the associated constraint is not active. It should be noted that all methods are robust with respect to the initial DoE and provide feasible solutions with respect to their RIs. As previously mentioned, it should be noted that all the 50 solutions obtained by each strategy are feasible. Tables 5 and 6 show that each SORA-based technique provides a solution close to the SORA-IS method. Each proposed modification does not affect the accuracy of the overall method with respect to the median value. Similarly to Table 2, the computational cost of the two-level approach, SORA, SORA-IS, B-SORA, B-SORA AS, and MFB-SORA is given in Table 7. The right column indicates the median and interquartile range of the ratio between the cost of each improved SORA strategy (over the 50 repetitions) and the cost of SORA from [46], taken as the reference.

It appears that each improvement of SORA leads to a reduction in the number of HF evaluations. BO in B-SORA reduces the cost by a factor of 2, BO in the augmented space in B-SORA AS by a factor of 6.2, and multifidelity in MFB-SORA reduces the total cost by a factor of 11.4. The robustness of the solution is also improved. As a conclusion, the effectiveness of MFB-SORA is demonstrated in the speed reducer case, showcasing its ability to offer a precise and resilient solution at an affordable computational cost.

D. Solid-Propellant Rocket Booster

1. *Description*

Solid-propellant rocket motors are often used in aerospace due to their high thrust. Indeed, they can be employed either as the main engine for the rocket (e.g., main core of Vega or Long March 11) or for side boosters such as for Ariane 6, Space Shuttle, and SLS. The design of a solid motor is quite complex because the delivered thrust

Table 5 Speed reducer case: RBDO solution for the two-level and the SORA and SORA-IS strategies, and median solution for B-SORA, B-SORA AS, and MFB-SORA computed over 50 repetitions[a]

Parameter	$f(\boldsymbol{q}_{\mathrm{opt}})$	$\boldsymbol{q}_{\mathrm{opt}}$						
Two-level	3031.33	[3.56,	0.7,	17.0,	7.3,	7.746,	3.36,	5.3]
SORA	3031.47	[3.56,	0.7,	17.0,	7.3,	7.747,	3.36,	5.3]
SORA-IS	3031.37	[3.56,	0.7,	17.0,	7.3,	7.747,	3.36,	5.3]
B-SORA	3031.39	[3.56,	0.7,	17.0,	7.3,	7.747,	3.36,	5.3]
	(2×10^{-2})	$(8 \times 10^{-6}$,	0,	7×10^{-7},	4×10^{-6},	4×10^{-4},	7×10^{-6},	$1 \times 10^{-5})$
B-SORA AS	3031.38	[3.56,	0.7,	17.0,	7.3,	7.747,	3.36,	5.3]
	(9×10^{-3})	$(5 \times 10^{-6}$,	0,	0,	0,	1×10^{-4},	7×10^{-6},	$3 \times 10^{-6})$
MFB-SORA	3031.38	[3.56,	0.7,	17.0,	7.3,	7.747,	3.36,	5.3]
	(8×10^{-3})	$(3 \times 10^{-5}$,	0,	0,	3×10^{-4},	8×10^{-6},	2×10^{-6},	$2 \times 10^{-6})$

[a]The first columns correspond to the median of the objective function value $f(\boldsymbol{q}_{\mathrm{opt}})$, and the last column provides their associated input values. Median values are indicated, and corresponding interquartile ranges are given in parentheses.

Table 6 Speed reducer case: reliability indices (RIs) for the two-level approach, SORA, SORA-IS, and for the median solution of each method B-SORA, B-SORA AS, and MFB-SORA[a]

Parameter	β_1	β_2	β_3	β_4	β_5	β_6	β_7	β_8	β_9	β_{10}	β_{11}
Two-level	—	—	—	—	3.0073	2.9958	—	2.9949	—	—	1.9967
SORA	—	—	—	—	2.9997	2.9990	—	2.9989	—	—	1.9996
SORA-IS	—	—	—	—	2.9999	2.9996	—	2.9998	—	—	2.0002
B-SORA	—	—	—	—	3.0003	3.0006	—	2.9999	—	—	2.0499
					(2×10^{-3})	(2×10^{-3})		(4×10^{-4})			(5×10^{-2})
B-SORA AS	—	—	—	—	3.0029	3.0003	—	2.9998	—	—	2.0005
					(2×10^{-3})	(6×10^{-4})		(2×10^{-4})			(2×10^{-2})
MFB-SORA	—	—	—	—	3.0014	2.9999	—	3.0003	—	—	2.0078
					(3×10^{-4})	(4×10^{-4})	—	(1×10^{-3})			(7×10^{-4})

[a]The RIs corresponding to the median values in Table 5 are indicated, and corresponding interquartile ranges are given in parentheses.

Table 7 Aerospace speed reducer case: computational cost of SORA, SORA-IS, the two-level approach, B-SORA, B-SORA AS, and MFB-SORA over 50 repetitions for LF and HF model evaluations and total cost[a]

Parameter	LF cost	HF cost	Total cost	Cost reduction (w.r.t. SORA)
Two-level	—	9×10^{10}	9×10^{10}	—
SORA	—	2195	2195	—
SORA-IS	—	4×10^{6}	4×10^{6}	—
B-SORA	—	**1020.0** (37.0)	**1020.0** (37.0)	∼**2.2**(0.1)
B-SORA AS	—	**354.0** (27.0)	**354.0** (27.0)	∼**6.2**(0.5)
MFB-SORA	**358.0** (28.0)	**156.0** (0.0)	**191.8** (3.0)	∼**11.4**(0.2)

[a]Median value and associated interquartile range are, respectively, given in bold and in parentheses. The right column indicates the median and interquartile range of the ratio between the cost of each proposed strategy and the cost of SORA.

directly results from the geometry of the propellant grain. Figure 7 describes several types of grain topology. Different geometries will lead to different thrust profiles (Fig. 8). Indeed, at a given time, the thrust is directly dependent on the burning surface inside the grain. Consequently, the design of the grain has to be performed accurately in order to ensure the performance of the engine in terms of thrust law. The mass flow rate $\dot{m}$ of a solid-propellant motor is given by the relation [72]:

$$\dot{m} = A_b r \rho_b$$

with A_b the burning area, r the burning rate, and ρ_b the propellant density. The thrust can be defined by the following equation:

$$T = \dot{m} v_e + (P_e - P_a)A_e = A_b r \rho_b v_e + (P_e - P_a)A_e$$

with T the thrust, v_e the exhaust velocity, P_e the nozzle exit pressure, P_a the atmospheric pressure, and A_e the nozzle exit area. For a large part of solid propellants, the burning rate can be defined by the following empirical formula [72]:

$$r = a p^n$$

with p the chamber pressure, a the burning rate coefficient, and n the burning rate exponent. The total impulse of the engine can be calculated by integrating the thrust over the time:

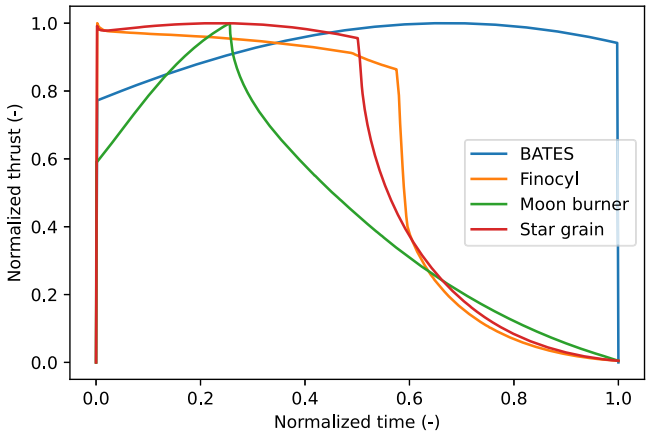

Fig. 8 Normalized thrust profiles for the grain geometries described in Fig. 7.

$$I = \int_{t0}^{t_f} T(t)\,\mathrm{d}t$$

All along the flight, the burning area A_b varies depending on the grain geometry and the burning rate. For example, variations of finocyl grain are depicted in Fig. 9. In this figure, the yellow region

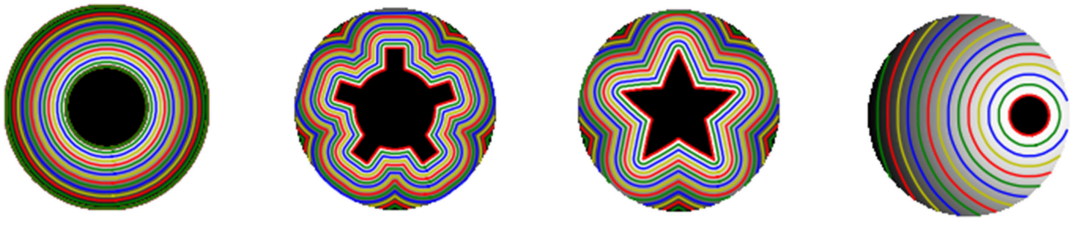

Fig. 7 Different types of grain. From the left to the right: Ballistic Test and Evaluation System (BATES), finocyl, star, and moon burners.

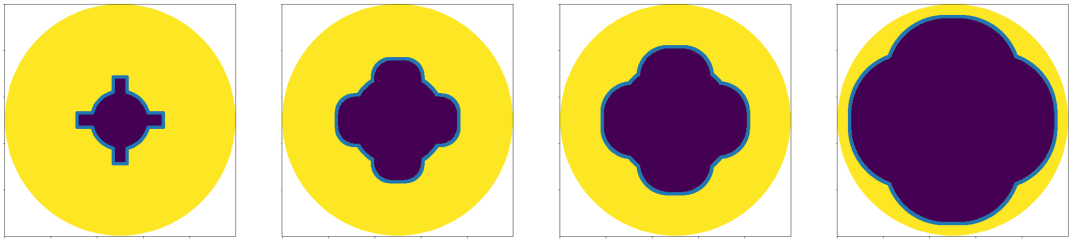

Fig. 9 Evolution of cross-sectional geometry along the time for a finocyl grain.

is the unburnt propellant, the light blue curve stands for the burning surface, and the dark blue region is the empty region.

In this test case, it is proposed to design a small solid rocket motor, using BATES geometry, and with TP-H-1202 as propellant [73]. This propellant is composed of 21% of aluminum, 57% of azide polymer, 12% of cyclotetramethylene tetranitramine (HMX), and 10% of hydroxy-terminated polybutadiene (HTPB). For that purpose, an RBDO problem involving four variables is solved. The objective of the design problem is to minimize the overall mass m of the propellant with a constraint relative to the delivered impulse. The different variables that are considered are the outer diameter of the grain $d_o \in [0.6, 1]$ (deterministic, in meters), the nozzle exit diameter $d_e \in [0.3, 0.5]$ (deterministic, in meters), the core diameter of the grain $d_c \in [0.1, 0.2]$ (mean of a controlled aleatory variable, in meters), and the propellant density $\rho_b \sim \mathcal{N}(1840, 184)$ (noncontrolled aleatory variable, in $\mathrm{kg/m^3}$). These variables are illustrated in Fig. 10. The considered uncertainty in the core diameter of the grain is due to the manufacturing process. We suppose that the standard deviation of this uncertainty is about 3 mm: $D_c \sim \mathcal{N}(d_c, 0.003)$. The uncertainty about the grain density is due to the chemical properties of the elements that compose the grain and the synthesis process. The resulting RBDO problem is

$$\min_{\boldsymbol{d},p} \; m(\boldsymbol{d}, p)$$
$$\text{s.t.} \quad \mathbb{P}[I(\boldsymbol{d}, X(p), Z) \leqslant I^t_{\text{target}}] \leqslant P^t_f$$

with $\boldsymbol{d} = \{d_o, d_e\}$, $p = \{d_c\}$, and $Z = \{\rho_b\}$. The mass (objective function) is calculated for a nominal value of ρ_b, whereas in the calculation of the impulse, it is supposed that variations of ρ_b can be involved. The target impulse I^t_{target} is equal to 1.5×10^3 kN · s. The failure probability threshold is equal to 1%. In order to compute the objective and constraint function, a propulsion code named** *openmotor* is used. This simulation code computes the geometrical evolution of the grain along the time and estimates the thrust and the overall impulse. High-fidelity and low-fidelity versions of the code have been derived in this test case. The low-fidelity involves some simplifications in the grain composition and a coarser time grid to simulate the evolution of the grain geometry (every 1 s instead of 0.1 s in the high-fidelity model).

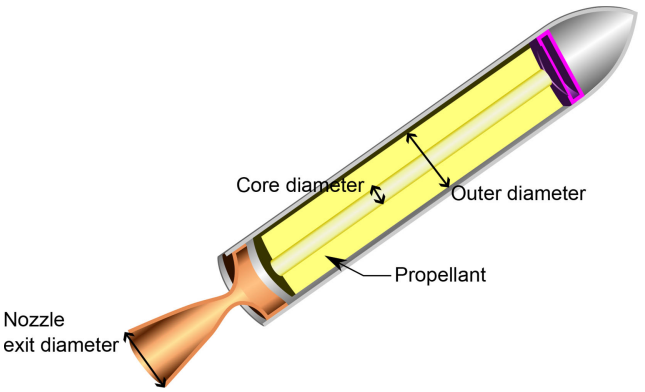

Fig. 10 Solid rocket motor with BATES geometry and considered variables.

**Data available online at https://github.com/reilleya/openMotor.

2. Results

The results obtained for this test case are described in this section. SORA, B-SORA, B-SORA AS, and MFB-SORA have been applied. Due to the computational cost of the simulation codes, 10 repetitions have been performed on this test case. The solutions found by the different methods are described in Table 8 and Fig. 11 (the gray dashed line represents the objective value of the solution of SORA). The grain mass found by all the methods is about 957 kg. The discrepancy between the different methods is about 500 g, which is very small compared to the overall propellant mass. All the methods converge to the same solution in terms of optimization variable values. Indeed, the optimal outer diameter is about 0.77 m, the nozzle exit diameter is 0.3 m, and the core diameter is about 0.2 m for all the methods.

The standard deviations of the optimal design variables are very low for this test case. It is lower than 0.1 mm for all the variables. Furthermore, the probability of failure at the optimum is equal to the target probability with a low standard deviation. Regarding the computational cost (Fig. 11 and Table 9), the same trends are observed: the use of a Bayesian version of SORA allows to decrease by 13.3 the computational cost with respect to SORA. The use of Bayesian SORA in augmented space allows to decrease by nearly 20 the computational cost. The latter is decreased by a factor of 34.6 by multifidelity Bayesian SORA. Furthermore, the computational cost due to the use of HF model goes from 70.0 with B-SORA-AS to 31.5 with MFB-SORA, which illustrates the benefit of multifidelity for this test case.

Figure 12 displays the distributions of mass and total impulse at the initialization of SORA and at the optimum. These distributions are shifted at the optimum. Indeed, the mass is decreased, and the distribution of impulse is sharper than at the initialization. The distribution shifts show the behavior of the optimization process that minimizes the overall mass while satisfying the constraint about the total impulse. Eventually, the dispersion of the thrust profiles at the initialization and at the optimum are given in Fig. 13. These curves have been obtained by Monte Carlo simulation using the high-fidelity code. The thrust curve at the optimum presents a larger level of thrust at the beginning of the flight, thus allowing the design constraint about the impulse (integral of the thrust) to be respected.

E. Sounding Rocket Design Problem

1. Description

The final test case deals with the optimization of a sounding rocket. Sounding rockets are suborbital launch vehicles frequently employed for scientific experiments that collect atmospheric data throughout their flights. The launch sequence is first composed of a powered phase, employing a single or multiple stages. Then, the sounding rocket undergoes a ballistic flight to reach its apogee. A reentry phase is finally executed to safely land either on the ground or in the sea (Fig. 14).

Figure 14 depicts the trajectory of a single-stage sounding rocket trajectory with an altitude at apogee of 300 km. During the trajectory, the fairing of the sounding rocket is jettisoned in order to perform the experimentation with the payload.

Table 8 Solid-propellant motor case: RBDO solution for SORA and median solution for B-SORA, B-SORA AS, and MFB-SORA computed over 10 repetitions[a]

	$f(\boldsymbol{q}_{\text{opt}})$		$\boldsymbol{q}_{\text{opt}}$		$P_{f,1}$
SORA	956.6	[0.769,	0.3,	0.2]	1.0×10^{-2}
B-SORA	957.2	[0.769,	0.3,	0.2]	1.0×10^{-2}
	(0.4)	(1.6×10^{-4}	5.3×10^{-12},	1.4×10^{-13})	(1.3×10^{-4})
B-SORA AS	957.7	[0.770,	0.3,	0.2]	1.0×10^{-2}
	(0.1)	(2.0×10^{-4},	5.3×10^{-9},	1.2×10^{-21})	(4.7×10^{-4})
MFB-SORA	956.7	[0.769,	0.3,	0.2]	1.0×10^{-2}
	(1.8)	(6.7×10^{-4}	4.8×10^{-7},	2.0×10^{-10})	(9.6×10^{-4})

[a]The first column corresponds to the median of the objective function value $f(\boldsymbol{q}_{\text{opt}})$, and the last columns provide their associated input and constraint values. Median values are indicated, and corresponding interquartile ranges are given in parentheses.

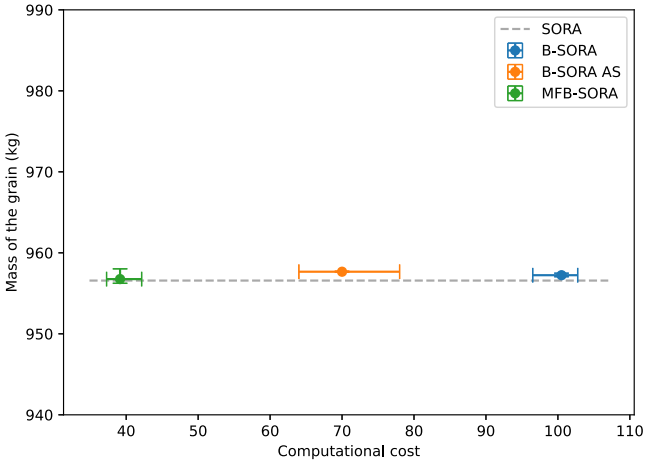

Fig. 11 Solid-propellant motor case. Objective function evaluated at the RBDO solution as a function of the computational cost for the 10 repetitions of each method.

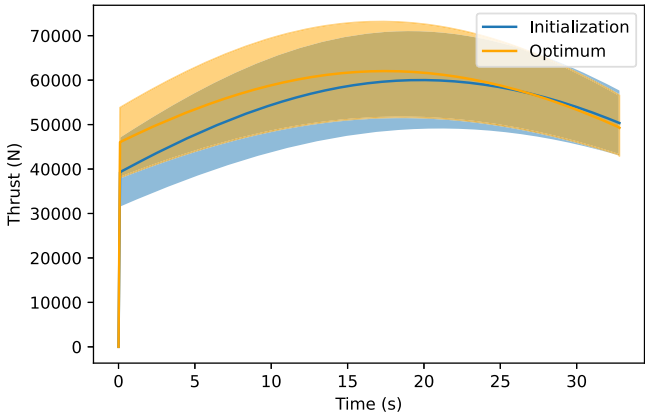

Fig. 13 Distributions of thrust as a function of time at the beginning of the SORA process (initialization) and at the final point (optimum). The mean curves are depicted in plain line. The filling areas represent the standard deviations around the mean curves.

Table 9 Solid-propellant motor case: computational cost of SORA, B-SORA, B-SORA AS, and MFB-SORA over 50 repetitions for LF and HF model evaluations and total cost[a]

Parameter	LF cost	HF cost	Total cost	Cost reduction (w.r.t. SORA)
SORA	— —	1331	1331	— —
B-SORA	— —	**100.5** (6.3)	**100.5** (6.3)	~**13.4** (0.8)
B-SORA AS	— —	**70.0** (14.0)	**70.0** (14.0)	~**19.6** (3.7)
MFB-SORA	**81.0** (29.0)	**31.5** (2.75)	**39.2** (4.9)	~**34.6** (4.1)

[a]Median value and associated interquartile range are, respectively, given in bold and in parentheses. The right column indicates the median and interquartile range of the ratio between the cost of each proposed strategy and the cost of SORA.

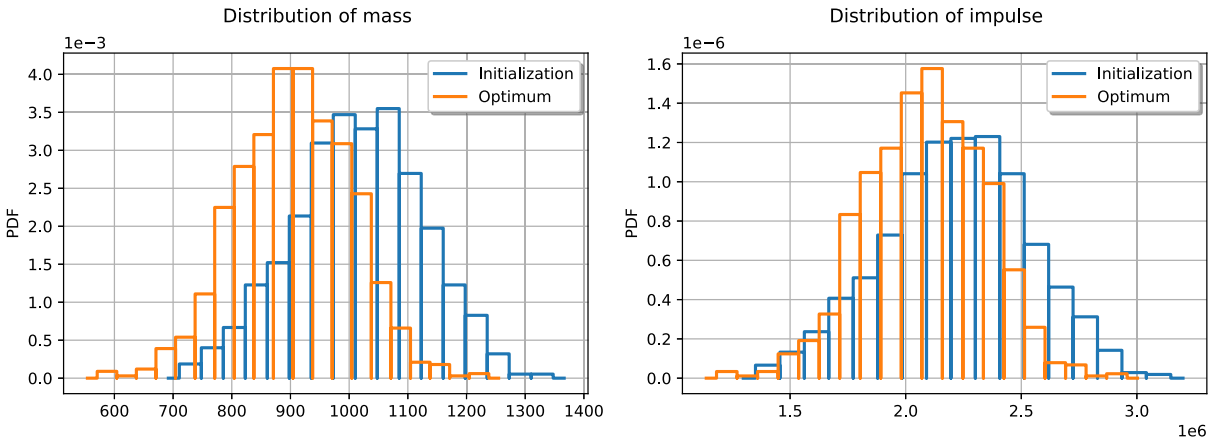

Fig. 12 Distributions of mass and impulse at the beginning of the SORA process (initialization) and at the final point (optimum).

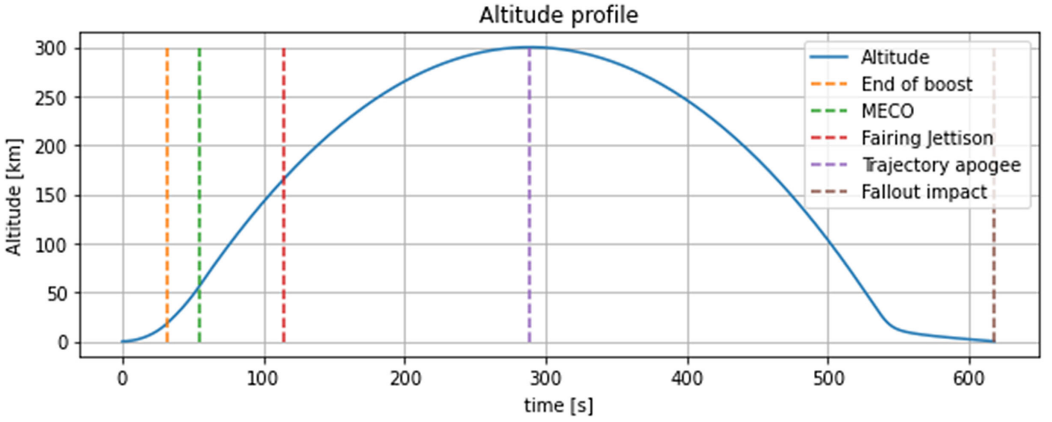

Fig. 14 Illustration of the sounding rocket trajectory (MECO, main engine cutoff).

This RBDO problem deals with a single-stage solid propellant sounding rocket, as shown in Fig. 15. This problem involves a solver based on a multidisciplinary process with four coupled disciplines: trajectory, aerodynamics, structure, and propulsion (Fig. 16) that interact using OpenMDAO [74].

The trajectory discipline aims to simulate the flight of the sounding rocket through the integration of the equations of motion, defined as follows:

$$f_{\text{ode}}: \begin{cases} \dot{r} = v\sin(\phi) \\ \dot{\lambda} = \frac{v\cos(\phi)}{r} \\ \dot{v} = \frac{-D+T\cos(\theta-\phi)}{m} + (-g+\omega^2 r)\sin(\phi) \\ \dot{\phi} = \frac{L}{mv} + \frac{T\sin(\theta-\phi)}{mv} + \frac{(\omega^2 r-g)\cos(\phi)}{v} + 2\omega + \frac{v\cos(\phi)}{r} \\ \dot{m} = -q \end{cases} \tag{24}$$

with ω the angular velocity of the Earth, λ the longitude of the launch vehicle, ϕ the flight path angle, r the position vector from the center of the Earth to the geometric center of the launch vehicle, α the angle of attack, m the current launcher mass, q the mass flow rate, g the acceleration of gravity, L the lift force, D the drag force, θ the pitch angle, T the thrust force, and v the velocity vector. To numerically integrate the trajectory, a Runge–Kutta algorithm is used with event handling to deal with the different phases of the trajectory (Fig. 14).

The purpose of the aerodynamics discipline is to assess the influence of the atmosphere during the launch vehicle flight by estimating the aerodynamic coefficients of the launcher for the different configurations (with and without fairing, engine on or off, ascent, or reentry). These estimations are challenging due to the different encountered Mach regimes (subsonic, transonic, supersonic, and hypersonic). In this study, the high-fidelity aerodynamics model is based on MISSILE [75]. It is a semi-empirical code allowing to assess the lift and drag coefficients as a function of vehicle geometry, orientation, and Mach number. The low-fidelity code uses a statistical formula calibrated with respect to expert knowledge (analytical model).

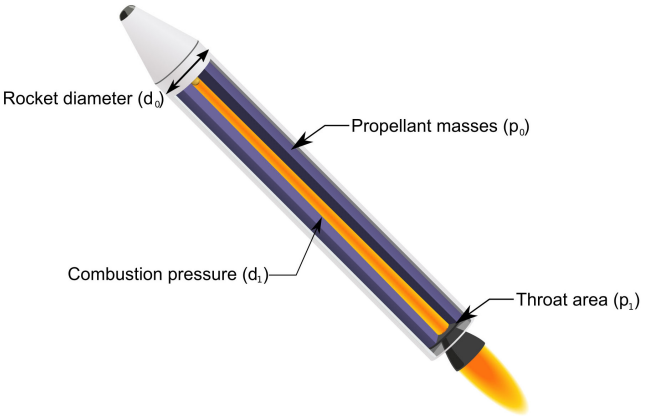

Fig. 15 Illustration of solid-propellant single-stage sounding rocket with the different design variables (d and p).

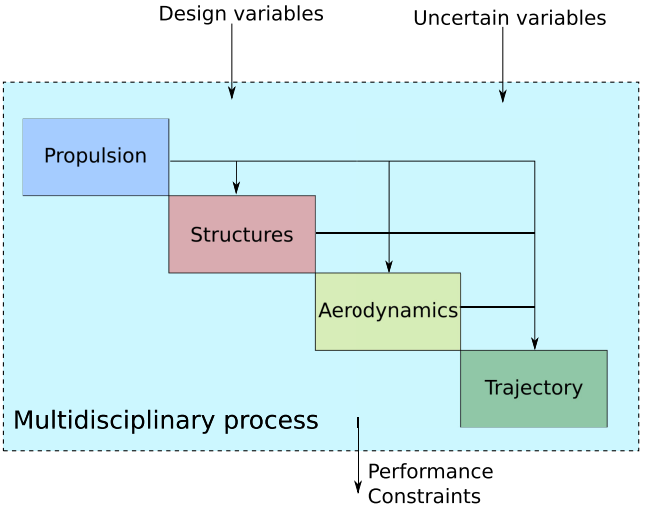

Fig. 16 Illustration of the multidisciplinary process of the sounding rocket test case.

The structure model combines simplified physical models for primary structures (e.g., tanks, skirt, thrust frame) and mass estimation relationships for secondary structures (e.g., avionics, thermal protection) [76]. This discipline takes as inputs the coupling variables from the other disciplines (e.g., propulsion, aerodynamics) and estimates the dry mass of the sounding rocket. The low-fidelity model for the structure involves a statistical relationship between the inert mass as a function of the propellant mass.

Eventually, the propulsion discipline is in charge of providing the thrust profile and the engine efficiency (specific impulse) based on classical rocket equations [73]. The isentropic coefficient at the throat, γ_t, the flame temperature T_c, and the molecular mass at combustion, M_c, are generated from standard data [72,73]. From these parameters, the characteristic velocity of the propellants (C^*) is determined:

$$C^* = \eta_c . \frac{\sqrt{\gamma_t . R . T_c}}{\gamma_t \left(\frac{2}{\gamma_t+1}\right)^{\frac{\gamma_t+1}{2(\gamma_t-1)}}}$$

with R the gas constant and η_c the combustion efficiency. From the isentropic coefficient and the pressure ratio Pc/Pe, the nozzle area ratio ϵ is given by

$$\epsilon = \frac{\left(\frac{2}{\gamma_t+1}\right)^{\frac{1}{\gamma_t-1}} \cdot \frac{Pc^{\frac{1}{\gamma_t}}}{Pe}}{\sqrt{\left(\frac{\gamma_t+1}{\gamma_t-1}\right) \cdot \left(1-\left(\frac{Pe}{Pc}\right)^{\frac{\gamma_t-1}{\gamma_t}}\right)}}$$

Finally, the specific impulse is given by

$$Isp = \lambda_n \cdot \frac{C^*}{g_0}\left(\gamma_t \sqrt{\left(\frac{2}{\gamma_t-1}\right) \cdot \left(\frac{2}{\gamma_t+1}\right)^{\frac{\gamma_t+1}{\gamma_t-1}} \cdot \left(1-\frac{Pe}{Pc}\right)^{\frac{\gamma_t-1}{\gamma_t}}} + \frac{\epsilon}{Pc}(Pe-P_a)\right)$$

with λ_n the nozzle efficiency and P_a the local atmospheric pressure.

Similar to the preceding test cases, two levels of fidelity (LF and HF) are available. The LF model involves simplifications in the aerodynamics and structure disciplines. The different fidelities of each function are denoted $\{f_{\text{LF}}(\cdot), f_{\text{HF}}(\cdot)\}$ and $\{g_{\text{LF}}(\cdot), g_{\text{HF}}(\cdot)\}$.

The objective of the sounding rocket is to carry out a scientific experiment at a given altitude $\text{alt}^t_{\text{apogee}}$ (here 250 km). It is then important to ensure, with a high level of confidence, the probability of reaching this target altitude at the apogee of the trajectory. The objective of the RBDO problem is then to optimize the flight performance by minimizing the gross liftoff weight (GLOW), while ensuring to reach a target altitude. The corresponding RBDO problem is

$$\min_{d_0,d_1,p_0,p_1} \text{GLOW}(d_0,d_1,p_0,p_1)$$
$$\text{s.t.} \quad \mathbb{P}[\text{alt}(d_0,d_1,\boldsymbol{X}(p_0,p_1),Z_0) \leqslant \text{alt}^t_{\text{apogee}}] \leqslant P^t_f$$

where $[d_0,d_1,p_0,p_1]^T$ is the design vector; d_0 and d_1, respectively, stand for the stage diameter (cm) and the combustion chamber pressure (MPa) for the solid rocket propulsion. The variables p_0 and p_1, respectively, denote the propellant mass (kg) and the throat area (cm^2) of the nozzle for the solid rocket engine. These variables are defined such that $d_0 \in [20,60]$, $d_1 \in [9,11]$, $p_0 \in [350,500]$, and $p_1 \in [10,25]$.

The variables X_0, X_1, and Z_0 are random variables distributed according to normal probability distributions such that $X_0 \sim \mathcal{N}(p_0, 0.1)$, $X_1 \sim \mathcal{N}(p_1, 0.25)$, and $Z_0 \sim \mathcal{N}(0, 0.1)$. The random variable X_0 describes the uncertainty in the final propellant mass available at liftoff, and X_1 is used to model the uncertainty in the throat area of the rocket engine due to the manufacturing process. The random variable Z_0 models the uncertainty in the drag parameter for the aerodynamics during the ascent phase. These uncertainties translate into uncertainties in the trajectories of the sounding rocket. Figure 17 depicts the dispersion of the rocket trajectories (using the LF and HF models) for 50 realizations of the random vector for a given design baseline. The apogee of each trajectory can be compared to the target altitude to be reached. In Fig. 17, it appears that the LF solver gives a similar trajectory to the HF solver, but with some discrepancies, especially at the apogee. Indeed, no LF trajectory reaches the target altitude.

The goal of the RBDO problem is to minimize the mass of the rocket at liftoff while ensuring that the probability of failing to reach the target altitude remains below a predetermined threshold $P^t_f = 0.001$.

2. Results

Table 10 presents the solution given by SORA as well as the median solution obtained for each advanced strategy over the 50 repetitions and its associated interquartile range (given between parentheses). As previously reported for the analytical test cases, the first column corresponds to the median of the objective function $f(\boldsymbol{q}_{\text{opt}})$, and the last columns provide the associated input and constraint values. Figure 18 depicts the optimal solutions obtained as a function of the computational cost over 50 repetitions for the three advanced SORA strategies (color-coded). The gray dashed line represents the objective value of the solution of SORA.

As summarized in Table 10, all methods provide the same solution. Indeed, the corresponding median objective function values differ from 0.02 kg at most and are feasible with respect to the probabilistic constraint. All the values of $P_{f,1}$ at the optimal solutions for the 50 repetitions of each method are smaller than the limit value $P^t_{f,1}$. As depicted in Fig. 18, working in the augmented space allows us to mitigate the dispersion of the results among the repetitions. The computational cost of the median solution and its

Table 10 Sounding rocket case: RBDO solution for SORA and median solution for B-SORA, B-SORA AS, and MFB-SORA computed over 50 repetitions[a]

Parameter	$f(\boldsymbol{q}_{\text{opt}})$	$\boldsymbol{q}_{\text{opt}}$				$P_{f,1}$
SORA	683.47	[51.1,	9.75,	438.0,	14.8]	1×10^{-3}
B-SORA	683.49	[51.3,	9.73,	438.2,	14.7]	9.7×10^{-4}
	(0.03)	(0.33,	0.09,	0.05,	0.30)	(1×10^{-5})
B-SORA AS	683.48	[51.0,	9.78,	437.9,	14.8]	9.9×10^{-4}
	(3×10^{-3})	(0.06,	0.06,	0.12,	0.03)	(7×10^{-7})
MFB-SORA	683.48	[51.2,	9.74,	438.0,	14.8]	9.8×10^{-4}
	(5×10^{-3})	(0.28,	0.03,	0.14,	0.04)	(2×10^{-6})

[a]The first column corresponds to the median of the objective function value $f(\boldsymbol{q}_{\text{opt}})$, and the last columns provide their associated input and constraint values. Median values are indicated, and corresponding interquartile ranges are given in parentheses.

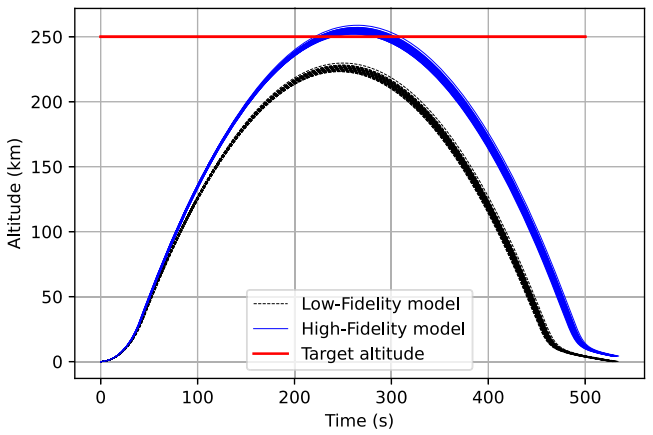

Fig. 17 Fifty realizations of the sounding rocket trajectories due to uncertainties, computed with the HF level (in blue) and the LF level (in black). The target altitude is represented in red (250 km).

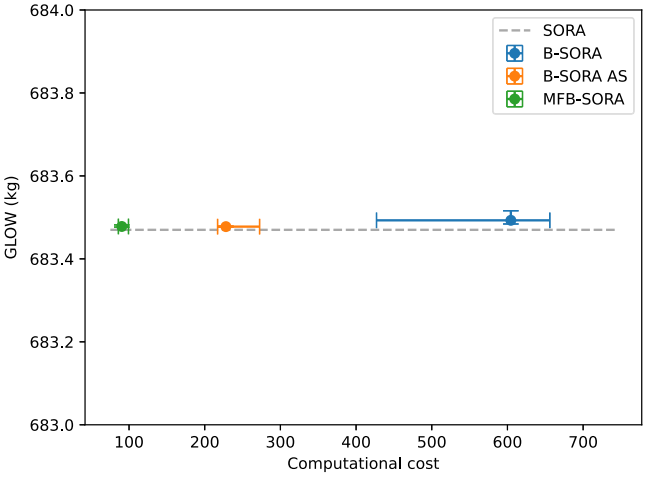

Fig. 18 Sounding rocket case. Objective function evaluated at the RBDO solution as a function of the computational cost for the 50 repetitions of each method.

dispersion (interquartile range) are also improved by each modification of SORA. More details about optimal solutions, constraint values, and computational costs obtained for the 50 repetitions are displayed in Fig. 19.

The results illustrated in Fig. 19 reinforce the conclusions given for this test case. This figure shows the dispersion of the results over the 50 repetitions in terms of optimal objective function value, constraint probability of failure (consequently, constraint violation rate), and computational cost. The dispersion of results in terms of optimal solution is reduced by working in the augmented space. Furthermore, each additional technique reduces calculation costs and dispersion over the 50 repetitions. Thanks to the contribution of multifidelity and the work in the augmented space, MFB-SORA allows us to obtain the most accurate results at the lowest computational cost. In addition, the proposed method provides solutions with a zero constraint violation rate over the 50 repetitions (all the values of the probability of failure are below the target probability of failure of 10^{-3}). With the B-SORA strategy, one solution violates the probabilistic constraint. This test case illustrates the efficiency and robustness to initialization of MFB-SORA, with a final result accurate with respect to the reference solution obtained by SORA.

The obtained trajectories are depicted in Fig. 20.

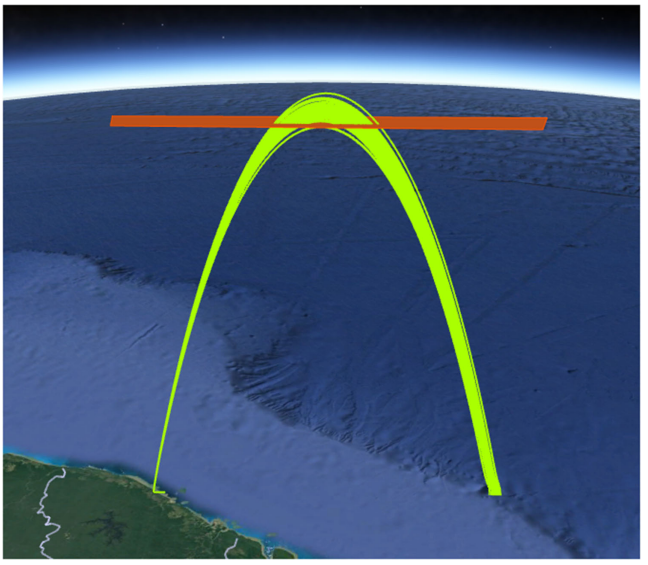

Fig. 20 Sounding rocket case. Illustration of trajectory dispersion at the optimum with the target threshold in red.

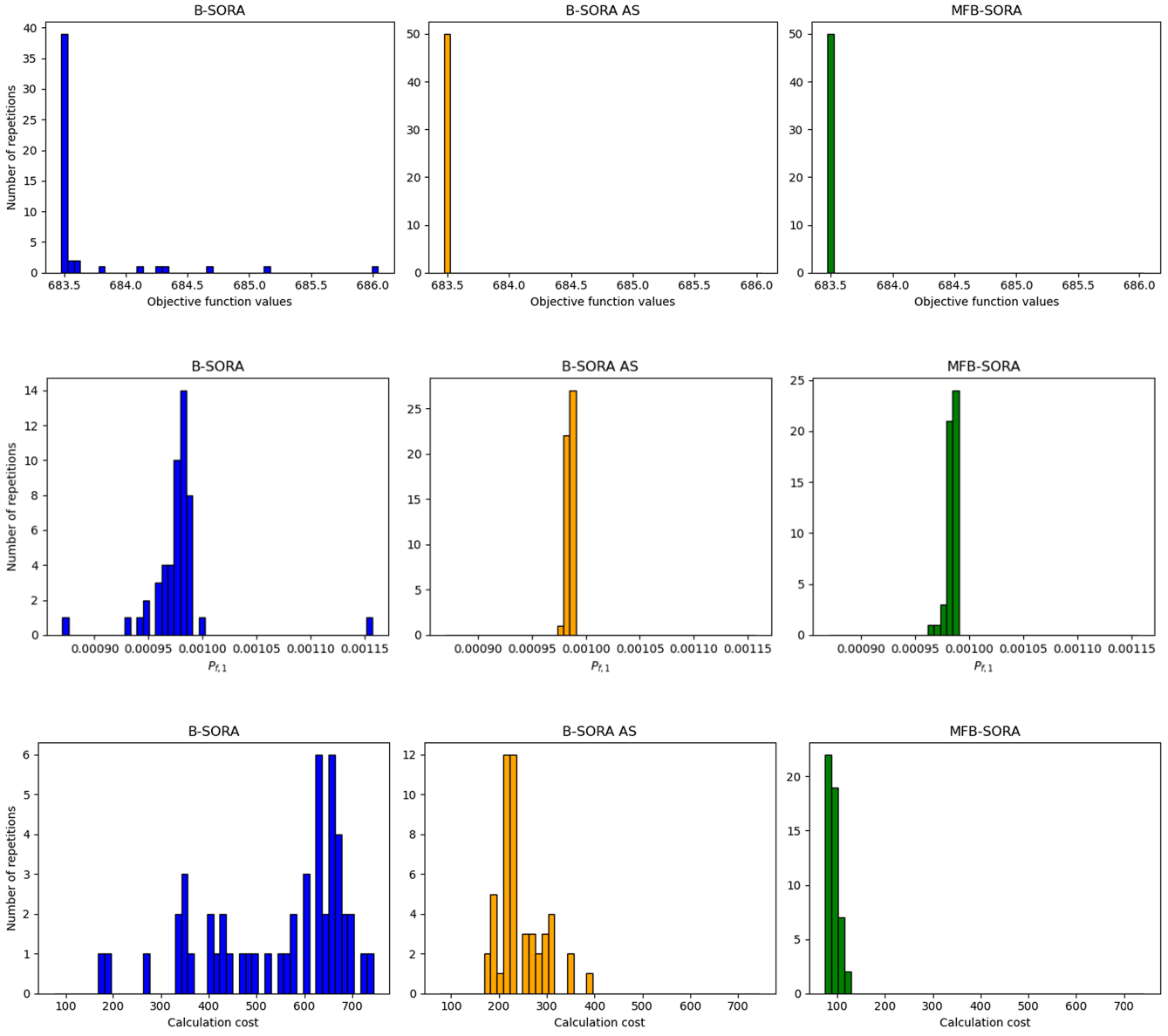

Fig. 19 Sounding rocket case. Histograms of objective function (top) and probabilistic constraint (middle) evaluated at the RBDO solution and computational cost (bottom) for the 50 repetitions of each method.

Table 11 Sounding rocket case: computational cost of SORA, SORA-IS, the two-level approach, B-SORA, B-SORA AS, and MFB-SORA over 50 repetitions for LF and HF model evaluations and total cost[a]

Parameter	LF cost	HF cost	Total cost	Cost reduction (w.r.t. SORA)
SORA	—	4054	4054	—
B-SORA	—	**605.0** (221.0)	**605.0** (221.0)	∼**6.7** (3.4)
B-SORA AS	—	**228.0** (57.0)	**228.0** (57.0)	∼**17.8** (3.6)
MFB-SORA	**226.0**(63.0)	**67.0** (10.0)	**90.4** (13.2)	∼**44.8** (6.3)

[a]Median value and associated interquartile range are, respectively, given in bold and in parentheses. The right column indicates the median and interquartile range of the ratio between the cost of each proposed strategy and the cost of SORA.

The computational cost of each advanced SORA is compared to that of SORA, taken as the reference, in Table 11. The right column indicates the median and interquartile range (in parentheses) of the ratio between the cost of each improved SORA strategy (over the 50 repetitions) and the cost of SORA.

Due to the complexity of the case and associated unaffordable calculations, neither the two-level approach nor the SORA-IS approach was implemented for this test case. Indeed, it is impossible to carry out a number of multidisciplinary process evaluations of the order of 10^7. The conclusions from the analytical test case remain: each modification of SORA allows to reduce the computational cost in terms of the number of HF model evaluations. The integration of Bayesian optimization in SORA with the B-SORA approach allows to reduce the median cost from 4054 to 605 HF model evaluations. In addition, using the augmented space (B-SORA AS), the global cost of SORA is divided by about 18 times. Finally, the introduction of multifidelity information sources with the MFB-SORA approach reduces the cost by about 45 times. It should be noted that the interquartile range of the SORA-based framework is also reduced in the advanced strategies from 221 to 13.2, proving the robustness of the method. This industrial test case allows us to illustrate the ability of MFB-SORA to reduce the computational cost while ensuring the accuracy of the optimal solution for a computationally expensive case study.

Furthermore, unlike the majority of previous test cases that address structural optimization, this application case allows to test the proposed MFB-SORA strategy on a multiphysics case involving structure, trajectory, and aerodynamics disciplines that are coupled into a multidisciplinary process. To evaluate the objective function and constraints, this test case involves structural, aerodynamic, and trajectory calculations.

V. Conclusions

The paper proposes a novel RBDO strategy based on SORA. The approach is composed of three distinct steps, allowing the reduction of the computational cost of SORA by replacing the expensive solvers with multifidelity surrogate models. The proposed framework uses surrogate models to replace the objective and constraint functions, thus enabling Bayesian optimization of the SORA suboptimization problems (involved in deterministic optimization and reliability analysis phases). The surrogate models are built in an augmented space along the SORA iteration process to optimally use the collected information along the iterations. Furthermore, the information from different fidelity levels is used to construct the surrogate models, through a multifidelity framework based on Gaussian Process. The proposed strategy is named MFB-SORA. The performance of the method has been assessed on five different test cases: three analytical cases involving physical problems and two cases based on industrial aerospace problems. The approach is compared to existing approaches of the literature. The proposed multifidelity RBDO approach, MFB-SORA, provides an optimal solution associated with a reduced computational cost compared to existing approaches while ensuring robustness of the solution to the initial Design of Experiments.

Future works could investigate alternative multifidelity surrogate model strategies beyond AR1 for test cases that present nonlinear dependencies between levels of fidelity. The combination of the proposed method with advanced Gaussian process modeling techniques dedicated to high-dimensional problems could be interesting to scale up the proposed approach to very high-dimensional test cases.

Furthermore, the proposed approach could be extended to solve multi-objective optimization problems under uncertainty. A key point would be linked to the resolution of the optimization subproblems in SORA with a dedicated Bayesian approach, in order to efficiently explore and exploit relevant regions of the Pareto front. Adaptive enrichment of surrogate models could be based on multi-objective acquisition criteria such as expected hypervolume improvement (EHVI) [77,78] and its multifidelity extension, for instance, by coupling EHVI with MF-MES (Max-value Entropy Search), as in [79].

Finally, another approach would be to integrate other Bayesian multifidelity optimization methods (e.g., [36,38,39]) into SORA to solve the optimization subproblems. It would then be possible to compare the efficiency and accuracy of the proposed MFB-SORA workflow with the integration of these methods.

Appendix A: Computational Settings and Test Case Description

A.1. Design of Experiments and Surrogate Modeling

The different strategies presented in this paper are implemented in `Python`. The package OpenTURNS [80] is used to define the distributions of the uncertain parameters. All the DoEs are constructed using a Latin hypercube sampling (LHS) using the pyDOE2 library [81]. The number of points M for the initial DoEs in single-fidelity is chosen such as $M = 4 \times d$, with d the dimension of the considered function. In the multifidelity case, the number of points for each fidelity to construct the multifidelity surrogate models is taken such as $M_{\mathrm{LF}} = M_{\mathrm{HF}} = 4 \times d$. A limited number of data points have been preferred to construct a first surrogate model. This latter is then enriched during the optimization. This point is discussed in [82].

The bounds taken to define the uncertain domain during the RA stage of SORA depend on the uncertain parameter distributions. In the different test cases, all the variables are modeled by a Gaussian distribution with parameters $\{\mu_i, \sigma_i\}_{i=1,\ldots,d}$, where d is the number of uncertain variables and μ_i corresponds either to the previous solution of the DO phase (for a controlled uncertain variable X), or to the mean of an uncontrolled variable Z. The bounds of the uncertain domain are then defined such that $[\mu_i - 3\sigma_i, \mu_i + 3\sigma_i]_{i=1,\ldots,d}$.

The standard and multifidelity GPs are constructed using the Surrogate Modeling Toolbox (`SMT`) package [83]. The covariance functions taken to define the GPs are squared exponential kernels. The nugget parameter is set to $\sigma^2 = 10^{-10}$ for the standard GPs, and $\sigma_\ell^2 = 10^{-10}$ with $\ell \in \{1, \ldots, L\}$ for the multifidelity GPs. The training process of each GP is performed by an integrated optimization solver (COBYLA) using 10 restarts. All the surrogate models in the Bayesian optimization problems have been constructed in a normalized space. For the stopping criterion of the BO processes, it is assumed that each optimization has converged when the norm of the distance between two consecutive selected points is less than 1×10^{-3} in the normalized space.

The library OpenTURNS [80] has been used for the optimization solvers. The LN_COBYLA solver has been used for the two-level approach for the analytical case, as well as for the DO and RA optimization problems in the classical SORA approach. It has been also used to optimize the acquisition function in the RA

subproblems for all the test cases. The two-level approach for the speed reducer case has been performed using the "pso_gen" solver of `Pagmo` in OpenTURNS.

A.2. Description of the Analytical Test Case

The analytical test case is composed of one objective function subject to two constraint functions, as follows:

$$\min_{d_0,p_0,p_1} f(d_0,p_0,p_1)$$
$$\text{s.t.} \begin{cases} \mathbb{P}[g_i(d_0,\boldsymbol{X}(p_0,p_1),Z_0)\leqslant 0]\leqslant P^t_{f,i} & \text{for } i=1,2 \\ -0.5\leqslant d_0,p_0,p_1\leqslant 2.5 \end{cases}$$

where two fidelity models (LF and HF) of each function $f(\cdot)$ and $g_i(\cdot)$ are considered, denoted by $\{f_{\text{LF}}(\cdot),f_{\text{HF}}(\cdot)\}$ and $\{g_{i,\text{LF}}(\cdot),g_{i,\text{HF}}(\cdot)\}_{i=1,2}$, such that

1) $$\begin{cases} f_{\text{HF}}(d_0,p_0,p_1)=2+(p_0-1.5)^2+(1.2-p_1d_0)^2+2(d_0-1.8)^2 \\ f_{\text{LF}}(d_0,p_0,p_1)=0.5f_{\text{HF}}(d_0,p_0,p_1)+2p_0-(1.2-p_1\times d_0)^2 \end{cases}$$

2) $$\begin{cases} g_{1,\text{HF}}(d_0,\boldsymbol{X}(p_0,p_1),Z_0)=1.0-d_0(X_0+1)+(\sqrt{Z_0}+2) \\ \quad +X_1-1.5 \\ g_{1,\text{LF}}(d_0,\boldsymbol{X}(p_0,p_1),Z_0)=2.5g_{1,\text{HF}}(d_0,\boldsymbol{X}(p_0,p_1),Z_0) \\ \quad -d_0(X_1+1) \end{cases}$$

3) $$\begin{cases} g_{2,\text{HF}}(d_0,\boldsymbol{X}(p_0,p_1),Z_0)=0.2(1+d_0)^2+X_1-Z_0+2.5 \\ g_{2,\text{LF}}(d_0,\boldsymbol{X}(p_0,p_1),Z_0)=0.2g_{2,\text{HF}}(d_0,\boldsymbol{X}(p_0,p_1),Z_0)+1 \\ \quad +d_0-Z_0 \end{cases}$$

In order to optimize the acquisition function in the DO part, the AUGLAG solver of `NLopt` in OpenTURNS has been used.

A.3. Description of the Vehicle Brake Disk Test Case

The vehicle brake disk case is composed of one objective function subject to one constraint function, as follows:

$$\min_{\mu_{h3}} f(\mu_{h3}) \qquad \text{s.t.} \begin{cases} \mathbb{P}[g(\boldsymbol{X}(\boldsymbol{p}),Z_u,Z_p)\leqslant 0]\leqslant P^t_f \\ \boldsymbol{p}=[\mu_{h1},\mu_{h2},\mu_{h3}] \\ 14.5\leqslant\mu_{h1}\leqslant 15.5 \\ 19.5\leqslant\mu_{h2}\leqslant 20.5 \\ 12\leqslant\mu_{h3}\leqslant 20 \end{cases}$$

where two fidelity models (LF and HF) of each function $f(\cdot)$ and $g(\cdot)$ are considered, denoted by $\{f_{\text{LF}}(\cdot),f_{\text{HF}}(\cdot)\}$ and $\{g_{\text{LF}}(\cdot),g_{\text{HF}}(\cdot)\}$, such that

1) $$\begin{cases} f_{\text{HF}}(p_3)=p_3 \\ f_{\text{LF}}(p_3)=0.5f_{\text{HF}}(p_3)+2/3 \end{cases}$$

2) $$\begin{cases} g_{1,\text{HF}}(\boldsymbol{X}(p_1,p_2,p_3),Z_u,Z_p)=g_{1,\text{LF}}(\boldsymbol{X}(p_1,p_2,p_3),Z_u,Z_p)+0.25p_1Z_p-1.15\frac{p_2}{p_3}-Z_u \\ g_{1,\text{LF}}(\boldsymbol{X}(p_1,p_2,p_3),Z_u,Z_p)=0.046287+0.20458Z_u-0.059821Z_p-0.00036549p_1 \\ -0.010037p_2+0.013836p_3+0.24308Z_uZ_p-0.0037884Z_up_1+0.0023358Z_up_2-0.016918Z_up_3 \\ +0.029287Z_pp_1-0.015872Z_pp_2-0.0028333Z_pp_3+0.0007175p_1p_2-0.00046158p_1p_3 \\ -0.0003648p_2p_3-0.39076Z_u^2-0.015968Z_p^2-0.0011936p_1^2+0.000269p_2^2+0.00062638p_3^2+0.01 \end{cases}$$

In order to optimize the acquisition function in the DO part, the LD_SLSQP solver of `NLopt` in OpenTURNS has been used.

A.4. Description of Speed Reducer Case

The third case is the speed reducer case, involving one objective function subject to 11 constraint functions, such that

$$\min_{p_1,\ldots,p_7} f(p_1,\ldots,p_7)$$
$$\text{s.t.} \begin{cases} \mathbb{P}[g_i(X_1(p_1),\ldots,X_7(p_7))>0]\leqslant P^t_{f,i} & \text{for } i=1,\ldots,11 \\ 2.6\leqslant p_1\leqslant 3.6 \\ 0.7\leqslant p_2\leqslant 0.8 \\ 17\leqslant p_3\leqslant 28 \\ 7.3\leqslant p_4,p_5\leqslant 8.3 \\ 2.9\leqslant p_6\leqslant 3.9 \\ 5\leqslant p_7\leqslant 5.5 \end{cases}$$

where two fidelity models (LF and HF) of each function $f(\cdot)$ and $g_i(\cdot)$ are considered, denoted by $\{f_{\text{LF}}(\cdot),f_{\text{HF}}(\cdot)\}$ and $\{g_{i,\text{LF}}(\cdot),g_{i,\text{HF}}(\cdot)\}_{i=1,\ldots,11}$, such that

1) $$f_{\text{HF}}(p_1,p_2,p_3,p_4,p_5,p_6,p_7)=0.7854p_1p_2^2(3.3333p_3^2+14.9334p_3-3.0934)-1.5080p_1(p_6^2+p_7^2)+7.4770(p_6^3+p_7^3)+0.7854(p_4p_6^2+p_5p_7^2)$$

2) $$g_{1,\text{HF}}(X_1(p_1),X_2(p_2),X_3(p_3))=27/(X_1X_2^2X_3)-1$$

3) $$g_{2,\text{HF}}(X_1(p_1),X_2(p_2),X_3(p_3))=397.5/(X_1X_2^2X_3^2)-1$$

4) $$g_{3,\text{HF}}(X_2(p_2),X_3(p_3),X_4(p_4),X_6(p_6))=1.93X_4^3/(X_2X_3X_6^4)-1$$

5) $$g_{4,\text{HF}}(X_2(p_2),X_3(p_3),X_5(p_5),X_7(p_7))=1.93X_5^3/(X_2X_3X_7^4)-1$$

6) $$g_{5,\text{HF}}(X_2(p_2),X_3(p_3),X_4(p_4),X_6(p_6))=\sqrt{(745X_4/(X_2X_3))^2+16.9\times 0^6}/(0.1X_6^3)-1100$$

7) $$g_{6,\text{HF}}(X_2(p_2),X_3(p_3),X_5(p_5),X_7(p_7))=\sqrt{(745X_5/(X_2X_3))^2+157.5\times 0^6}/(0.1X_7^3)-850$$

8) $$g_{7,\text{HF}}(X_2(p_2),X_3(p_3))=X_2X_3-40$$

9) $$g_{8,\text{HF}}(X_1(p_1),X_2(p_2))=5-X_1/X_2$$

10) $$g_{9,\text{HF}}(X_1(p_1),X_2(p_2))=X_1/X_2-12$$

11) $$g_{10,\text{HF}}(X_4(p_4),X_6(p_6))=(1.5X_6+1.9)/X_4-1$$

12) $$g_{11,\text{HF}}(X_5(p_5),X_7(p_7))=(1.1X_7+1.9)/X_5-1$$

As presented in the paper, this case is derived in multifidelity by introducing LF models such that $\boldsymbol{h}_{\text{LF}}(\boldsymbol{x})=\boldsymbol{\alpha}\times\boldsymbol{h}_{\text{HF}}(\boldsymbol{x})+\boldsymbol{\eta}$. The vectors $\boldsymbol{\alpha}$ and $\boldsymbol{\eta}$ (of size 12 and chosen randomly) and the vectors

$\boldsymbol{\beta}^t$ (of size 11) and $\boldsymbol{\sigma}$ (of size 7) introduced before are defined such that

1) $\boldsymbol{\alpha} = [2., 2.5, -0.8, 3.1, 0.7, 0.5, -0.5, 0.9, -1.7, 1.8, 1.1, 2.4]^T$

2) $\boldsymbol{\eta} = [-1, 0, -1.2, 3.6, 1, 2.9, 2.2, 3.7, -3.9, 52.2, 0, -2.6]^T$

3) $\boldsymbol{\beta}^t = [3, 2, 3, 3, 3, 3, 2, 3, 2, 3,2]^T$

4) $\boldsymbol{\sigma} = [0.003, 0.004, 0.002, 0.003, 0.005, 0.004, 0.005]^T$

To optimize the acquisition function in the DO part, the LD_SLSQP solver of `NLopt` in OpenTURNS has been used.

A.5. Solid-Propellant Rocket Booster

To optimize the acquisition function in the DO part, the LD_SLSQP solver of `NLopt` in OpenTURNS has been used for this test case.

A.6. Sounding Rocket Case

To optimize the acquisition function in the DO part, the LD_MMA solver of `NLopt` in OpenTURNS has been used for this test case.

Acknowledgments

The authors thank M. Glen Sire (ONERA) for the development of the sounding rocket test case. This work is supported by a Ph.D. thesis funded by ONERA and CERFACS.

References

[1] Balesdent, M., Brevault, L., Paluch, B., Thépot, R., Wuilbercq, R., Subra, N., Defoort, S., Bourgaie, M., and Vieille, B., "Multidisciplinary Design and Optimization of Winged Architectures for Reusable Launch Vehicles," *Acta Astronautica*, Vol. 211, Oct. 2023, pp. 97–115. https://doi.org/10.1016/j.actaastro.2023.05.041

[2] Zolla, P. M., Rosa, R., Migliorino, M. T., and Bianchi, D., "Multi-Disciplinary Optimization of Single-Stage Hybrid Rockets for Lunar Ascent," *Acta Astronautica*, Vol. 222, Sept. 2024, pp. 493–507. https://doi.org/10.1016/j.actaastro.2024.06.026

[3] Mauriello, T., Wilken, J., Callsen, S., Bussler, L., and Sippel, M., "Multidisciplinary Design Analysis and Optimization of the Aerodynamic Shape of the SpaceLiner Passenger Stage," *Acta Astronautica*, Vol. 224, Nov. 2024, pp. 244–265. https://doi.org/10.1016/j.actaastro.2024.07.054

[4] Aldaghma, L., Muresan, D., and Renaud, S., "Establishing the Requirements for Safe Rocket Launches with Respect to Weather," *Acta Astronautica*, Vol. 213, Dec. 2023, pp. 392–407. https://doi.org/10.1016/j.actaastro.2023.07.008

[5] Aoues, Y., and Chateauneuf, A., "Benchmark Study of Numerical Methods for Reliability-Based Design Optimization," *Structural and Multidisciplinary Optimization*, Vol. 41, No. 2, 2010, pp. 277–294. https://doi.org/10.1007/s00158-009-0412-2

[6] Moustapha, M., and Sudret, B., "Surrogate-Assisted Reliability-Based Design Optimization: A Survey and a Unified Modular Framework," *Structural and Multidisciplinary Optimization*, Vol. 60, No. 5, 2019, pp. 2157–2176. https://doi.org/10.1007/s00158-019-02290-y

[7] Tu, J., Choi, K., and Park, Y. H., "A New Study on Reliability-Based Design Optimization," *Journal of Mechanical Design*, Vol. 121, No. 4, 1999, pp. 557–564. https://doi.org/10.1115/1.2829499

[8] Liang, J., Mourelatos, Z. P., and Tu, J., "A Single-Loop Method for Reliability-Based Design Optimization," *International Design Engineering Technical Conferences and Computers and Information in Engineering Conference*, Vol. 46946, Jan. 2004, pp. 419–430. https://doi.org/10.1115/DETC2004-57255

[9] Du, X., and Chen, W., "Sequential Optimization and Reliability Assessment Method for Efficient Probabilistic Design," *Journal of Mechanical Design*, Vol. 126, No. 2, 2004, pp. 225–233. https://doi.org/10.1115/1.1649968

[10] Yao, W., Chen, X., Luo, W., Van Tooren, M., and Guo, J., "Review of Uncertainty-Based Multidisciplinary Design Optimization Methods for Aerospace Vehicles," *Progress in Aerospace Sciences*, Vol. 47, No. 6, 2011, pp. 450–479. https://doi.org/10.1016/j.paerosci.2011.05.001

[11] Breitung, K., "Asymptotic Approximations for Multinormal Integrals," *Journal of Engineering Mechanics*, Vol. 110, No. 3, 1984, pp. 357–366. https://doi.org/10.1061/(ASCE)0733-9399(1984)110:3(357)

[12] Maier, H. R., Lence, B. J., Tolson, B. A., and Foschi, R. O., "First-Order Reliability Method for Estimating Reliability, Vulnerability, and Resilience," *Water Resources Research*, Vol. 37, No. 3, 2001, pp. 779–790. https://doi.org/10.1029/2000WR900329

[13] Ji, J., Zhang, C., Gao, Y., and Kodikara, J., "Reliability-Based Design for Geotechnical Engineering: An Inverse FORM Approach for Practice," *Computers and Geotechnics*, Vol. 111, July 2019, pp. 22–29. https://doi.org/10.1016/j.compgeo.2019.02.027

[14] Moustapha, M., and Sudret, B., "Quantile-Based Optimization Under Uncertainties Using Bootstrap Polynomial Chaos Expansions," *12th International Conference on Structural Safety and Reliability (ICOSSAR 2017)*, 2017, pp. 1561–1569.

[15] Lehký, D., Slowik, O., and Novák, D., "Reliability-Based Design: Artificial Neural Networks and Double-Loop Reliability-Based Optimization Approaches," *Advances in Engineering Software*, Vol. 117, March 2018, pp. 123–135. https://doi.org/10.1016/j.advengsoft.2017.06.013

[16] Dubourg, V., Sudret, B., and Bourinet, J.-M., "Reliability-Based Design Optimization Using Kriging Surrogates and Subset Simulation," *Structural and Multidisciplinary Optimization*, Vol. 44, No. 5, 2011, pp. 673–690. https://doi.org/10.1007/s00158-011-0653-8

[17] Moustapha, M., Sudret, B., Bourinet, J.-M., and Guillaume, B., "Quantile-Based Optimization Under Uncertainties Using Adaptive Kriging Surrogate Models," *Structural and Multidisciplinary Optimization*, Vol. 54, No. 6, 2016, pp. 1403–1421. https://doi.org/10.1007/s00158-016-1504-4

[18] Zhang, J., Xiao, M., and Gao, L., "A New Local Update-Based Method for Reliability-Based Design Optimization," *Engineering with Computers*, Vol. 37, No. 4, 2021, pp. 3591–3603. https://doi.org/10.1007/s00366-020-01019-6

[19] Jones, D. R., Schonlau, M., and Welch, W. J., "Efficient Global Optimization of Expensive Black-Box Functions," *Journal of Global Optimization*, Vol. 13, No. 4, 1998, pp. 455–492. https://doi.org/10.1023/A:1008306431147

[20] Rasmussen, C. E., and Williams, C. K., *Gaussian Processes for Machine Learning*, Vol. 1, Springer–Verlag, Berlin, 2006, pp. 63–71. https://doi.org/10.7551/mitpress/3206.001.0001

[21] Goovaerts, P., *Geostatistics for Natural Resources Evaluation*, Oxford Univ. Press, Oxford, 1997. https://doi.org/10.1093/oso/9780195115383.001.0001

[22] Morio, J., Balesdent, M., Jacquemart, D., and Vergé, C., "A Survey of Rare Event Simulation Methods for Static Input–Output Models," *Simulation Modelling Practice and Theory*, Vol. 49, Dec. 2014, pp. 287–304. https://doi.org/10.1016/j.simpat.2014.10.007

[23] Echard, B., Gayton, N., Lemaire, M., and Relun, N., "A Combined Importance Sampling and Kriging Reliability Method for Small Failure Probabilities with Time-Demanding Numerical Models," *Reliability Engineering & System Safety*, Vol. 111, March 2013, pp. 232–240. https://doi.org/10.1016/j.ress.2012.10.008

[24] Bichon, B. J., McFarland, J. M., and Mahadevan, S., "Efficient Surrogate Models for Reliability Analysis of Systems with Multiple Failure Modes," *Reliability Engineering & System Safety*, Vol. 96, No. 10, 2011, pp. 1386–1395. https://doi.org/10.1016/j.ress.2011.05.008

[25] Bect, J., Ginsbourger, D., Li, L., Picheny, V., and Vazquez, E., "Sequential Design of Computer Experiments for the Estimation of a Probability of Failure," *Statistics and Computing*, Vol. 22, No. 3, 2012, pp. 773–793. https://doi.org/10.1007/s11222-011-9241-4

[26] Marelli, S., and Sudret, B., "An Active-Learning Algorithm that Combines Sparse Polynomial Chaos Expansions and Bootstrap for Structural Reliability Analysis," *Structural Safety*, Vol. 75, Nov. 2018, pp. 67–74. https://doi.org/10.1016/j.strusafe.2018.06.003

[27] Moustapha, M., Marelli, S., and Sudret, B., "Active Learning for Structural Reliability: Survey, General Framework and Benchmark," *Structural Safety*, Vol. 96, May 2022, Paper 102174. https://doi.org/10.1016/j.strusafe.2021.102174

[28] Dessena, G., Ignatyev, D. I., Whidborne, J. F., and Fragonara, L. Z., "A Global–Local Meta-Modelling Technique for Model Updating,"

Computer Methods in Applied Mechanics and Engineering, Vol. 418, Jan. 2024, Paper 116511. https://doi.org/10.1016/j.cma.2023.116511

[29] Qian, J., Cheng, Y., Zhang, J., Liu, J., and Zhan, D., "A Parallel Constrained Efficient Global Optimization Algorithm for Expensive Constrained Optimization Problems," *Engineering Optimization*, Vol. 53, No. 2, 2021, pp. 300–320. https://doi.org/10.1080/0305215X.2020.1722118

[30] Au, S., "Reliability-Based Design Sensitivity by Efficient Simulation," *Computers & Structures*, Vol. 83, No. 14, 2005, pp. 1048–1061. https://doi.org/10.1016/j.compstruc.2004.11.015

[31] Alvarez, M. A., Rosasco, L., and Lawrence, N. D., "Kernels for Vector-Valued Functions: A Review," *Foundations and Trends® in Machine Learning*, Vol. 4, No. 3, 2012, pp. 195–266. https://doi.org/10.1561/2200000036

[32] Kennedy, M. C., and O'Hagan, A., "Predicting the Output from a Complex Computer Code When Fast Approximations Are Available," *Biometrika*, Vol. 87, No. 1, 2000, pp. 1–13. https://doi.org/10.1093/biomet/87.1.1

[33] Perdikaris, P., Raissi, M., Damianou, A., Lawrence, N. D., and Karniadakis, G. E., "Nonlinear Information Fusion Algorithms for Data-Efficient Multi-Fidelity Modelling," *Proceedings of the Royal Society A: Mathematical, Physical and Engineering Sciences*, Vol. 473, No. 2198, 2017, Paper 20160751. https://doi.org/10.1098/rspa.2016.0751

[34] Brevault, L., Balesdent, M., and Hebbal, A., "Overview of Gaussian Process Based Multi-Fidelity Techniques with Variable Relationship Between Fidelities, Application to Aerospace Systems," *Aerospace Science and Technology*, Vol. 107, Dec. 2020, Paper 106339. https://doi.org/10.1016/j.ast.2020.106339

[35] Lin, Q., Hu, J., Zhou, Q., Cheng, Y., Hu, Z., Couckuyt, I., and Dhaene, T., "Multi-Output Gaussian Process Prediction for Computationally Expensive Problems with Multiple Levels of Fidelity," *Knowledge-Based Systems*, Vol. 227, Sept. 2021, Paper 107151. https://doi.org/10.1016/j.knosys.2021.107151

[36] Meliani, M., Bartoli, N., Lefebvre, T., Bouhlel, M.-A., Martins, J. R., and Morlier, J., "Multi-Fidelity Efficient Global Optimization: Methodology and Application to Airfoil Shape Design," *AIAA Aviation 2019 forum*, AIAA Paper 2019-3236, 2019. https://doi.org/10.2514/6.2019-3236

[37] Korondi, P. Z., Marchi, M., Parussini, L., and Poloni, C., "Multi-Fidelity Design Optimisation Strategy Under Uncertainty with Limited Computational Budget," *Optimization and Engineering*, Vol. 22, No. 2, 2021, pp. 1039–1064. https://doi.org/10.1007/s11081-020-09510-1

[38] Song, J., Chen, Y., and Yue, Y., "A General Framework for Multi-Fidelity Bayesian Optimization with Gaussian Processes," *22nd International Conference on Artificial Intelligence and Statistics*, PMLR, 2019, pp. 3158–3167.

[39] Di Fiore, F., and Mainini, L., "Non-Myopic Multipoint Multifidelity Bayesian Framework for Multidisciplinary Design," *Scientific Reports*, Vol. 13, No. 1, 2023, Paper 22531. https://doi.org/10.1038/s41598-023-48757-3

[40] Chaudhuri, A., Marques, A. N., Lam, R., and Willcox, K. E., "Reusing Information for Multifidelity Active Learning in Reliability-Based Design Optimization," *AIAA Scitech 2019 Forum*, AIAA Paper 2019-1222, 2019. https://doi.org/10.2514/6.2019-1222

[41] Yoo, K., Bacarreza, O., and Aliabadi, M. F., "A Novel Multi-Fidelity Modelling-Based Framework for Reliability-Based Design Optimisation of Composite Structures," *Engineering with Computers*, Vol. 38, No. 1, 2022, pp. 1–14. https://doi.org/10.1007/s00366-020-01084-x

[42] Li, M., and Wang, Z., "Reliability-Based Multifidelity Optimization Using Adaptive Hybrid Learning," *ASCE-ASME Journal of Risk and Uncertainty in Engineering Systems, Part B: Mechanical Engineering*, Vol. 6, No. 2, 2020, Paper 021005. https://doi.org/10.1115/1.4044773

[43] Chaudhuri, A., Marques, A. N., and Willcox, K., "MfEGRA: Multifidelity Efficient Global Reliability Analysis Through Active Learning for Failure Boundary Location," *Structural and Multidisciplinary Optimization*, Vol. 64, No. 2, 2021, pp. 797–811. https://doi.org/10.1007/s00158-021-02892-5

[44] Liu, X., Deng, J., Chen, H., Zhai, G., and Wu, J., "An Efficient and Multi-Fidelity Reliability-Based Design Optimization Method Based on a Novel Surrogate Model Local Update Strategy," *Computer Methods in Applied Mechanics and Engineering*, Vol. 430, Oct. 2024, Paper 117219. https://doi.org/10.1016/j.cma.2024.117219

[45] Xia, B., Lü, H., Yu, D., and Jiang, C., "Reliability-Based Design Optimization of Structural Systems Under Hybrid Probabilistic and Interval Model," *Computers & Structures*, Vol. 160, Nov. 2015, pp. 126–134. https://doi.org/10.1016/j.compstruc.2015.08.009

[46] Chen, Z., Li, X., Chen, G., Gao, L., Qiu, H., and Wang, S., "A Probabilistic Feasible Region Approach for Reliability-Based Design Optimization," *Structural and Multidisciplinary Optimization*, Vol. 57, No. 1, 2018, pp. 359–372. https://doi.org/10.1007/s00158-017-1759-4

[47] Meng, Z., Li, G., Wang, X., Sait, S. M., and Yıldız, A. R., "A Comparative Study of Metaheuristic Algorithms for Reliability-Based Design Optimization Problems," *Archives of Computational Methods in Engineering*, Vol. 28, No. 3, 2021, pp. 1853–1869. https://doi.org/10.1007/s11831-020-09443-z

[48] Song, K., Zhang, Y., Zhuang, X., Yu, X., and Song, B., "Reliability-Based Design Optimization Using Adaptive Surrogate Model and Importance Sampling-Based Modified SORA Method," *Engineering with Computers*, Vol. 37, No. 2, 2021, pp. 1295–1314. https://doi.org/10.1007/s00366-019-00884-0

[49] Nikolaidis, E., and Burdisso, R., "Reliability Based Optimization: A Safety Index Approach," *Computers & Structures*, Vol. 28, No. 6, 1988, pp. 781–788. https://doi.org/10.1016/0045-7949(88)90418-X

[50] Mahadevan, S., "Monte Carlo Simulation," *Reliability-Based Mechanical Design*, Marcel Dekker Inc., New-York, 1997, pp. 123–146. https://doi.org/10.1017/cbo9780511809231.011

[51] Lee, J.-O., Yang, Y.-S., and Ruy, W.-S., "A Comparative Study on Reliability-Index and Target-Performance-Based Probabilistic Structural Design Optimization," *Computers & Structures*, Vol. 80, Nos. 3–4, 2002, pp. 257–269. https://doi.org/10.1016/S0045-7949(02)00006-8

[52] Wu, H.-C., "The Karush-Kuhn-Tucker Optimality Conditions in an Optimization Problem with Interval-Valued Objective Function," *European Journal of Operational Research*, Vol. 176, No. 1, 2007, pp. 46–59. https://doi.org/10.1016/j.ejor.2005.09.007

[53] Lin, C. D., and Tang, B., "Latin Hypercubes and Space-Filling Designs," *Handbook of Design and Analysis of Experiments*, CRC Press, Boca Raton, FL, 2015, pp. 593–625. https://doi.org/10.1201/b18619-27

[54] Tokdar, S. T., and Kass, R. E., "Importance Sampling: A Review," *Wiley Interdisciplinary Reviews: Computational Statistics*, Vol. 2, No. 1, 2010, pp. 54–60. https://doi.org/10.1002/wics.56

[55] Le Gratiet, L., and Garnier, J., "Recursive Co-Kriging Model for Design of Computer Experiments with Multiple Levels of Fidelity," *International Journal for Uncertainty Quantification*, Vol. 4, No. 5, 2014, pp. 365–386. https://doi.org/10.1615/Int.J.UncertaintyQuantification.2014006914

[56] Močkus, J., "On Bayesian Methods for Seeking the Extremum," *Optimization Techniques IFIP Technical Conference*, Springer–Verlag, Berlin, July 1974, pp. 400–404. https://doi.org/10.1007/978-3-662-38527-2_55

[57] Jones, D. R., "A Taxonomy of Global Optimization Methods Based on Response Surfaces," *Journal of Global Optimization*, Vol. 21, No. 4, 2001, pp. 345–383. https://doi.org/10.1023/A:1012771025575

[58] Žilinskas, A., "A Review of Statistical Models for Global Optimization," *Journal of Global Optimization*, Vol. 2, No. 2, 1992, pp. 145–153. https://doi.org/10.1007/BF00122051

[59] Auer, P., "Using Confidence Bounds for Exploitation-Exploration Trade-Offs," *Journal of Machine Learning Research*, Vol. 3, No. Nov, 2002, pp. 397–422.

[60] Srinivas, N., Krause, A., Kakade, S. M., and Seeger, M., "Gaussian Process Optimization in the Bandit Setting: No Regret and Experimental Design," arXiv preprint arXiv: 0912.3995, 2009.

[61] Wang, X., Jin, Y., Schmitt, S., and Olhofer, M., "Recent Advances in Bayesian Optimization," *ACM Computing Surveys*, Vol. 55, No. 13s, 2023, pp. 1–36. https://doi.org/10.1145/3582078

[62] Parr, J. M., Keane, A. J., Forrester, A. I., and Holden, C. M., "Infill Sampling Criteria for Surrogate-Based Optimization with Constraint Handling," *Engineering Optimization*, Vol. 44, No. 10, 2012, pp. 1147–1166. https://doi.org/10.1080/0305215X.2011.637556

[63] Audet, C., Denni, J., Moore, D., Booker, A., and Frank, P., "A Surrogate-Model-Based Method for Constrained Optimization," *8th*

Symposium on Multidisciplinary Analysis and Optimization, AIAA Paper 2000-4891, 2000.
https://doi.org/10.2514/6.2000-4891

[64] Tran, A., Tranchida, J., Wildey, T., and Thompson, A. P., "Multi-Fidelity Machine-Learning with Uncertainty Quantification and Bayesian Optimization for Materials Design: Application to Ternary Random Alloys," *Journal of Chemical Physics*, Vol. 153, No. 7, 2020, Paper 074705.
https://doi.org/10.1063/5.0015672

[65] Zhang, S., Lyu, W., Yang, F., Yan, C., Zhou, D., Zeng, X., and Hu, X., "An Efficient Multi-Fidelity Bayesian Optimization Approach for Analog Circuit Synthesis," *56th Annual Design Automation Conference 2019*, 2019, pp. 1–6.
https://doi.org/10.1145/3316781

[66] Huang, H., Liu, Z., Zheng, H., Xu, X., and Duan, Y., "A Proportional Expected Improvement Criterion-Based Multi-Fidelity Sequential Optimization Method," *Structural and Multidisciplinary Optimization*, Vol. 66, No. 2, 2023, p. 30.
https://doi.org/10.1007/s00158-022-03484-7

[67] Shu, L., Jiang, P., and Wang, Y., "A Multi-Fidelity Bayesian Optimization Approach Based on the Expected Further Improvement," *Structural and Multidisciplinary Optimization*, Vol. 63, No. 4, 2021, pp. 1709–1719.
https://doi.org/10.1007/s00158-020-02772-4

[68] Takeno, S., Fukuoka, H., Tsukada, Y., Koyama, T., Shiga, M., Takeuchi, I., and Karasuyama, M., "Multi-Fidelity Bayesian Optimization with Max-Value Entropy Search and Its Parallelization," *International Conference on Machine Learning*, PMLR, 2020, pp. 9334–9345.

[69] Kandasamy, K., Dasarathy, G., Oliva, J., Schneider, J., and Poczos, B., "Multi-Fidelity Gaussian Process Bandit Optimisation," *Journal of Artificial Intelligence Research*, Vol. 66, Sept. 2019, pp. 151–196.
https://doi.org/10.1613/jair.1.11288

[70] Le Gratiet, L., "Multi-Fidelity Gaussian Process Regression for Computer Experiments," Ph.D. Thesis, Univ. Paris-Diderot-Paris VII, Paris, France, 2013.

[71] Ravi, K., Fediukov, V., Dietrich, F., Neckel, T., Buse, F., Bergmann, M., and Bungartz, H.-J., "Multi-Fidelity Gaussian Process Surrogate Modeling for Regression Problems in Physics," *Machine Learning: Science and Technology*, Vol. 5, No. 4, 2024, Paper 045015.

[72] Sutton, G. P., and Biblarz, O., *Rocket Propulsion Elements*, Wiley, Hoboken, NJ, 2011.
https://doi.org/10.1016/0029-5582(63)90239-6

[73] Humble, R., Henry, G., and Larson, W., *Space Propulsion Analysis and Design*, College Custom Series, McGraw-Hill, New York, 1995.

[74] Gray, J. S., Hwang, J. T., Martins, J. R. R. A., Moore, K. T., and Naylor, B. A., "OpenMDAO: An Open-Source Framework for Multidisciplinary Design, Analysis, and Optimization," *Structural and Multidisciplinary Optimization*, Vol. 59, No. 4, 2019, pp. 1075–1104.
https://doi.org/10.1007/s00158-019-02211-z

[75] Denis, P., "ONERA's Aerodynamic Prediction Code- MISSILE," *RTO/AGARD, Symposium on Missile Aerodynamics*, Sorrento, Italy, ONERA, TP, May 1998.

[76] Castellini, F., "Multidisciplinary Design Optimization for Expendable Launch Vehicles," Ph.D. Thesis, Politecnico di Milano, Italy, 2012.

[77] Emmerich, M. T., "Single-and Multi-Objective Evolutionary Design Optimization Assisted by Gaussian Random Field Metamodels," Ph.D. Thesis, Dortmund Univ., Germany, 2005.

[78] Daulton, S., Balandat, M., and Bakshy, E., "Differentiable Expected Hypervolume Improvement for Parallel Multi-Objective Bayesian Optimization," *Advances in Neural Information Processing Systems*, Vol. 33, 2020, pp. 9851–9864.

[79] Irshad, F., Karsch, S., and Döpp, A., "Expected Hypervolume Improvement for Simultaneous Multi-Objective and Multi-Fidelity Optimization," arXiv preprint arXiv: 2112, Vol. 10, 2021.

[80] Baudin, M., Dutfoy, A., Iooss, B., and Popelin, A.-L., "OpenTURNS: An Industrial Software for Uncertainty Quantification in Simulation," *Handbook of Uncertainty Quantification*, Springer–Verlag, Berlin, 2017, pp. 2001–2038.
https://doi.org/10.1007/978-3-319-12385-1

[81] Sjögren, R., and Svensson, D., "pydoe2: An Experimental Design Package for Python," 2018, https://github. com/clicumu/pyDOE2.

[82] Le Riche, R., and Picheny, V., "Revisiting Bayesian Optimization in the Light of the COCO Benchmark," *Structural and Multidisciplinary Optimization*, Vol. 64, No. 5, 2021, pp. 3063–3087.
https://doi.org/10.1007/s00158-021-02977-1

[83] Bouhlel, M. A., Hwang, J. T., Bartoli, N., Lafage, R., Morlier, J., and Martins, J. R., "A Python Surrogate Modeling Framework with Derivatives," *Advances in Engineering Software*, Vol. 135, Sept. 2019, Paper 102662.
https://doi.org/10.1016/j.advengsoft.2019.03.005

M. J. Kochenderfer
Associate Editor